Determination of the water content and D/H ratio of the martian mantle by unraveling degassing and crystallization effects in nakhlites

A.H. Peslier [a,*], R. Hervig [b], S. Yang [c], M. Humayun [c], J.J. Barnes [d,e], A.J. Irving [f], A.D. Brandon [g]

[a] Jacobs, NASA-Johnson Space Center, Mail Code X13, Houston, TX 77058, USA
[b] School of Earth and Space Exploration, Arizona State University, Tempe, AZ 85287, USA
[c] National High Magnetic Field Lab, Florida State University, Tallahassee, FL 32310, USA
[d] ARES, NASA-Johnson Space Center, Houston, TX 77058, USA
[e] Lunar and Planetary Laboratory, University of Arizona, Tucson, AZ 85721, USA
[f] Dept. of Earth & Space Sciences, University of Washington, Seattle, WA, USA
[g] Dept. of Earth and Atmospheric Sciences, University of Houston, Houston, TX 77204, USA

Abstract

Knowing the distribution and origin of water in terrestrial planets is crucial to understand their formation, evolution and the source of their atmospheres and surface water. The nakhlites represent a suite of minimally shocked meteorites that likely originated from lava flows from a single volcano or from a shallow intrusion or sill complex on Mars. Measuring the water contents and D/H ratios of their igneous minerals allows identification of phases that have preserved their magmatic hydrogen, and therefrom permits estimation of the water content of their mantle source. Pyroxene, olivine, melt inclusions and mesostasis of five nakhlites (NWA 998, Nakhla, Y 000593, MIL 03346 and NWA 6148) were analyzed in situ for water contents and H isotopes, and major and trace element contents. No water was detected in olivine grains except in Y 000593. The water content of pyroxenes is highly heterogeneous within individual grains and between grains within a single meteorite. Water concentrations in pyroxene (<0.1–387 ppm H_2O), melt inclusions (26–4130 ppm H_2O) and mesostasis (1130–7850 ppm H_2O) decrease with increasing δD (from -268 to 4858‰) in all nakhlites.

After ruling out significant influence from spallation, exchange with the martian atmosphere, shock, surface alteration, and hydrothermal processes, the H data of the pyroxenes can be explained by degassing and crystallization processes. Degassing is consistent with a decrease of water content from pyroxene interior to edge. Fractionation of H isotopes during degassing results in increases of δD during H loss from pyroxene but in decreases in δD during H_2O-OH loss from a melt. Consequently, the low-water content, high-δD of most pyroxenes is best explained by degassing after the pyroxenes had crystallized. All melt and plagioclase inclusions analyzed are located in degassed pyroxenes and are also degassed. The lower δD of the mesostasis (24 ± 131‰) compared to that of the least-degassed pyroxenes (430 ± 172‰) is likely the result of melt degassing and interaction with hydrothermal fluids.

Magmatic H, however, has been preserved in each nakhlite in some pyroxenes that are characterized by >15 ppm H_2O and $\delta D < 700$‰. The H composition of the least-degassed, most-Mg-rich augites can be interpreted in two ways. If Cl-bearing hydrothermal fluids were assimilated by the parent magma of nakhlites prior to pyroxene crystallization, the H composition could represent a crustal signature. If hydrothermal fluid assimilation occurred after pyroxenes start crystallizing, it could be a mantle signature. We favor the latter scenario, in which case the martian mantle sampled by the nakhlites is estimated to con-

---

* Corresponding author.
 E-mail address: anne.h.peslier@nasa.gov (A.H. Peslier).

tain 59–184 ppm H_2O and to have a δD of 430 ± 172‰. These water contents, similar to those of the upper part of the terrestrial mantle, represent those of a shallow depleted martian mantle reservoir. The two to four times higher δD of the martian mantle relative to that of Earth could have resulted from the two planets acquiring their water from different proportions and types of carbonaceous chondrite-like planetesimals.

1. INTRODUCTION

Estimating the abundance and distribution of water in the martian mantle and thereby of the entire planet is the ultimate goal of studying hydrogen (H) and other volatiles in martian meteorites. Knowing how much water Mars originally held has implications for determining the distribution of water in the Solar System and thereby would constrain our models of planetary formation and the origin of water in terrestrial planets (Drake, 2005; Albarède, 2009; Peslier, 2010; Halliday, 2013; Alexander, 2017; Hallis, 2017; Peslier et al., 2017; Sharp, 2017b). Moreover, H isotopes can help pinpoint the source material that brought volatiles to Mars (e.g., Alexander, 2017). Water also played a role in the geological evolution of Mars given that H influences melting, deformation and thermal properties of rocks and melts (Mackwell et al., 1985; Hofmeister, 2004; Médard and Grove, 2006; Morschhauser et al., 2011; Pommier et al., 2012; Kiefer and Li, 2016). In turn, this has consequences for our understanding of the origin and composition of the martian atmosphere, ice and probable liquid water on its surface, and thereby the potential for life on the planet (Farmer et al., 1976; Bibring et al., 2004; Elkins-Tanton, 2008; Carr and Head, 2010; Cockell et al., 2012; Lammer et al., 2013; Usui et al., 2015).

Because no human or robotic mission has brought back samples from Mars, we only have meteorites, raising concerns on the effect of shock, surface processes and space exposure on the measured water contents and hydrogen isotopes. Moreover, the search of the amount and origin of water in the interior of Mars has been hampered by the fact that martian meteorites are all from the crust (McSween, 2015), resulting in weakly-constrained calculations to estimate the water content of the martian mantle. Nakhlites may be the best candidates we have to test and sort out these various processes in order to evaluate mantle water contents. The similarity in nakhlite crystallization ages (~1.3 Ga), their cosmic ray exposure ages (~11 My), and their compositions suggest that they may represent samples from one single area on Mars and that nakhlites were ejected by one impact event (e.g., Nyquist et al., 2001; Mikouchi et al., 2003; Treiman, 2005; Park et al., 2009; Korochantseva et al., 2011; McCubbin et al., 2013). It is exceptional for meteorites, to have several samples from the same volcanic area, perhaps the same outcrop, as opposed to other martian meteorites which likely each come from different areas. These clinopyroxene-rich mafic rocks are thought to be cumulates from various depths of either thick lava flows or a sill (Bunch and Reid, 1975; Reid and Bunch, 1975; Treiman, 2005; Lentz et al., 2011;

Richter et al., 2016; Jambon et al., 2016; Cohen et al., 2017, Udry and Day, 2018). Another advantage of nakhlites is that they are the least shocked of all martian meteorites having only sustained <20 GPa shock pressures (Fritz et al., 2005a,b; Treiman and Irving, 2008; Day et al., 2006; Jambon et al., 2016), mitigating the concern that their H may have been affected significantly by impact processes.

The D/H ratio of martian meteorites has been used to identify interactions between two end-members, a martian mantle reservoir and one or two surficial reservoirs. Here the D/H ratios are expressed in ‰ in the delta notation relative to the Vienna standard mean ocean water (VSMOW, with $(D/H)_{VSMOW} = 1.5576 \times 10^{-4}$; Gonfiantini, 1978):

$$\delta D = 1000 \times \left(\frac{(D/H)_{sample}}{(D/H)_{VSMOW}} - 1 \right) \qquad (1)$$

The martian mantle likely has low δD (<500‰) and surface reservoirs have high δD, likely inherited from interaction with the martian atmosphere that has a δD of 4950‰ (Owen et al., 1988; Webster et al., 2013; Villanueva et al., 2015) or from an ancient crustal reservoir with a δD of 1000–2000‰ (Usui et al., 2015). As a comparison, the δD of the Earth's mantle is estimated at ≤−100‰ (Deloule et al., 1991; Bell and Ihinger, 2000; Shaw et al., 2012; Hallis et al., 2015; Peslier et al., 2017). Terrestrial contamination (decreasing δD towards 0‰) and epoxy contamination during sample preparation (increasing water contents, decreasing δD) complicate the interpretations of martian meteorite H analyses (Boctor et al., 2003; Mane et al., 2016; Hallis et al., 2017). Hydrogen isotope analyses of most shergottite phases evidence interaction with surficial reservoirs (Boctor et al., 2003; Usui et al., 2012, 2015; Hu et al., 2014; Chen et al., 2015; Giesting et al., 2015; Mane et al., 2016; Hallis et al., 2017; Liu et al., 2018). An exception is the one melt inclusion from Yamato 980459, the most primitive olivine-phyric shergottite known, with the lowest δD (275 ± 10‰) measured in a martian melt inclusion. It is so far considered the closest estimate for the martian mantle δD (Usui et al., 2012). Estimations of the water content of the martian mantle vary from <75 parts per million by weight (ppm) H_2O for the shergottite sources (Usui et al., 2012; McCubbin et al., 2016) to 130–250 ppm H_2O for the source of Chassignites (McCubbin et al., 2010).

Work on H in nakhlites and chassignites, martian dunites that may be related to nakhlites (McCubbin et al., 2013; Udry and Day, 2018), has so far reported D/H analyses of bulk-rocks that indicate surface interaction with the martian atmosphere (Leshin et al., 1996), and volatile analyses of apatites showing that nakhlites were infiltrated by

Cl-rich hydrothermal fluids prior to their complete crystallization (Hallis et al., 2012a; McCubbin et al., 2013). One question in the nakhlite-chassignite suite is whether the interaction with surficial Cl-rich fluid occurred in the magma chamber prior to nakhlite pyroxene crystallization, or later after emplacement as magmatic flow or shallow intrusion. If the former, nakhlites will record crustal δD, if the latter, they could potentially be used to infer the δD of the martian mantle.

Here, five well-characterized nakhlites were selected. In order of slowest to fastest cooled, these are: North West Africa (NWA) 998 (Treiman and Irving, 2008), Nakhla (Bunch and Reid, 1975; Harvey and McSween, 1992; Wadhwa and Crozaz, 1995), Yamato (Y) 000593 (Mikouchi et al., 2003; Imae et al., 2005; Wadhwa et al., 2004), Miller Range (MIL) 03346 (Day et al., 2006; Hallis and Taylor, 2011; Udry et al., 2012) and NWA 6148 (paired with NWA 5790; Jambon et al., 2016; Balta et al., 2017). Hydrogen isotope ratios, along with water, major- and trace-element contents, were measured in pyroxene, olivine, melt inclusions and mesostasis using systematic in situ analyses of mineral grains to search for the presence or absence of co-variations. From these data, the processes that distributed water contents and D/H ratios in nakhlite phases are elucidated, and the dominance of degassing and crystallization processes is evidenced. Despite the multiple processes that could affect the distribution and isotopic composition of hydrogen in a meteorite from Mars, we show that some pyroxenes in nakhlites preserved igneous water contents and may have recorded mantle δD.

2. METHODS

Hand-separated nakhlite phases were doubly-polished without the use of any glue, oil or water. Mineral grains were then analyzed in sequence by several techniques, starting with the least destructive one, Fourier transform infrared spectrometry (FTIR, to measure water content and speciation), followed by electron microprobe (to analyze major element contents), secondary ion mass spectrometry (SIMS, to measure water contents and D/H ratios, Fig. SI1), scanning electron microscope (SEM, to examine the SIMS craters), and finally laser-ablation inductively-coupled plasma mass spectrometry (LA-ICPMS, to analyze trace element contents). As much as possible, the same locations were analyzed in situ on the same minerals with each technique, or nearby each location (i.e., LA-ICP-MS analysis done directly in the SIMS crater or within 50 μm of the SIMS crater). Details can be found in supplementary information (SI) 2.

3. RESULTS

3.1. FTIR OH spectra

All pyroxenes analyzed, except one in NWA 6148, have small OH bands barely distinguishable from the baseline (Fig. 1A). The OH bands are pleochroic, i.e. change in height when the infrared polarizer is rotated, testifying that this H is intrinsic to the pyroxene and located in its mineral defects (as opposed to liquid or gas in inclusions; Libowitzky and Beran, 2006). Characteristic pyroxene OH bands are at ~3620 (only in NWA 6148 and Y 000593), ~3515 and ~3450 cm^{-1}. These bands are at similar wavenumbers to those in terrestrial clinopyroxene (Skogby et al., 1990). No OH bands could be detected when the infrared polarizer was oriented parallel to the optical axes α or β in NWA 998, Nakhla and Y 000593 pyroxenes. The pyroxenes in MIL 03346 also had OH bands at 3650 and 3730 cm^{-1}, which could be due to amphibole inclusions (Libowitzky and Beran, 2004). It should be emphasized that nakhlite pyroxenes are not clear, i.e. gem quality, and typically contain abundant microscopic inclusions, and a clear path for the infrared beam could not always be found. One pyroxene from NWA 6148 (Px7, Fig. 1A) has OH bands unlike any other pyroxene measured by FTIR in this study: a large OH band is located at 3700–3000 cm^{-1} with sharp peaks emerging at ~3570 and ~3400 cm^{-1}. The latter OH bands are generally found in olivine, yet the major element composition measured by electron microprobe (Table SI1) as well as the Si—O— bands detected by FTIR definitely characterize that grain as an augite. The minimum water contents calculated from FTIR data range from below detection limit (<0.5 ppm H$_2$O) to 13 ppm H$_2$O in the nakhlite pyroxenes.

No OH bands were detected in olivines from NWA 998, Nakhla, MIL 03346 and NWA 6148 (Fig. 1C). The three olivine grains analyzed from Y 000593, however, exhibit a wide OH band between 3600 and 3000 cm^{-1} that is pleochroic but does not have the characteristic olivine OH bands (e.g., at 3571, 3400 cm^{-1}; e.g., Miller et al., 1987; Beran and Libowitzky, 2006). The exception is a band at ~3180 cm^{-1} that could be the expression of a hydrated Mg-vacancy in olivine, typically found at 3165 cm^{-1} in forsteritic mantle olivine (Lemaire et al., 2004; Berry et al., 2005). The overall spectrum is likely caused by H-bearing inclusions in Y 000593 olivines. The olivines of Y 000593 are full of μm size inclusions that could not be avoided during FTIR analysis (Fig. SI6B) and that were identified as clinopyroxene by EDX, consistent with previous findings (augite according to Imae et al., 2005; clinopyroxene-magnetite symplectites according to Mikouchi et al., 2003). On the other hand, such inclusions are present in Nakhla olivines too and yet no water was detected.

Analysis by FTIR of the mesostasis is hampered by its opacity resulting from its multi-phase characteristics. A thin (~25 μm) slice of the mesostasis from NWA 6148 had clearer area which analysis resulted in a large OH band between 3700 and 3000 cm^{-1} (Fig. 1B). Sharp peaks at 3568 and 3400 cm^{-1} may be caused by intrinsic H in olivine. No quantitative estimate of the water content is possible from these spectra, however, because multiple phases were analyzed and FTIR absorption spectra are thickness and mineral composition specific.

3.2. Water contents and H isotopes

In all nakhlites, the SIMS data exhibit a trend from high water content (thousands of ppm H$_2$O) and low δD (<200‰), in the mesostasis and one melt inclusion but also in a few pyroxene grains, to low water contents (<10 ppm
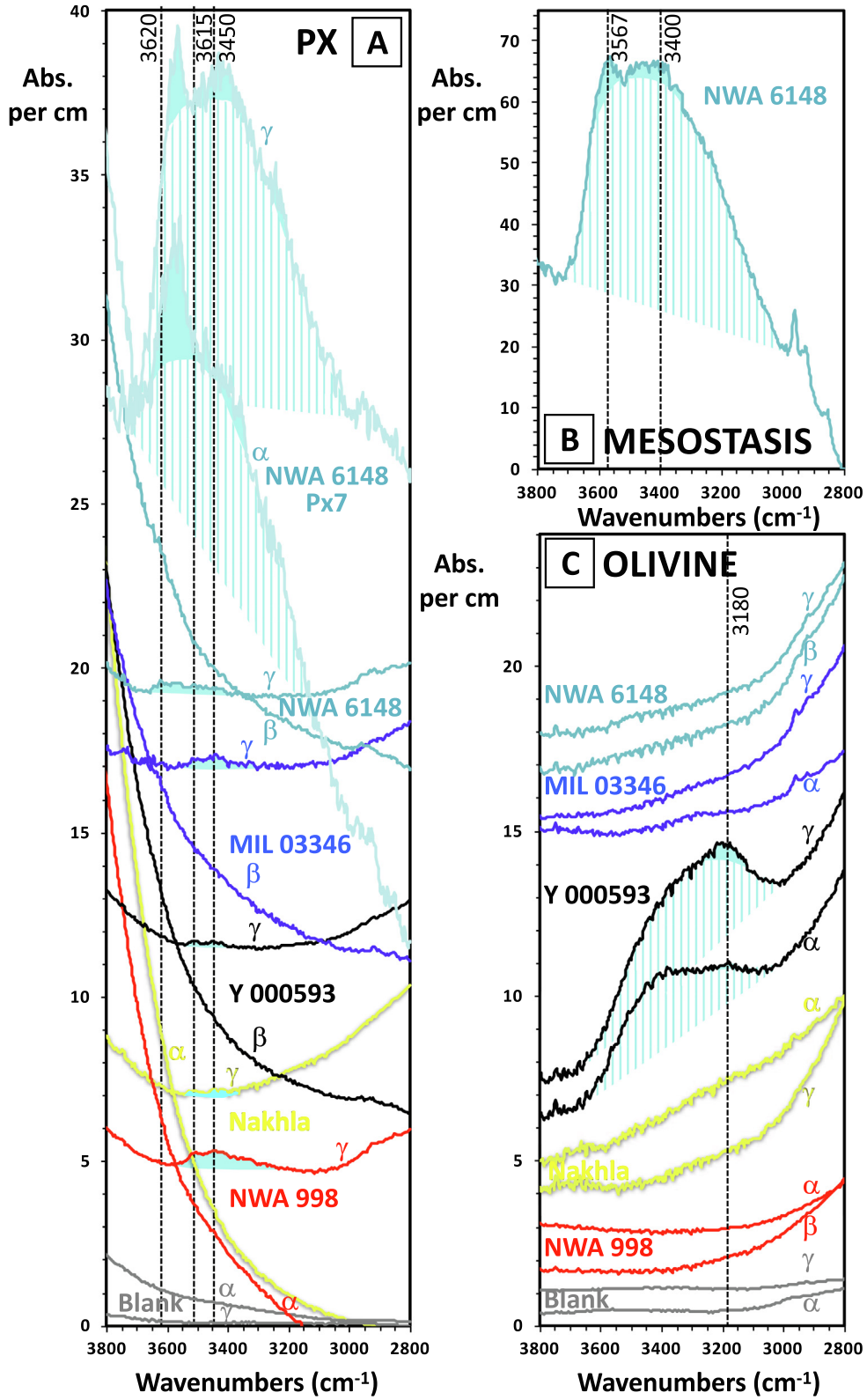
H_2O) and high δD ($\geq 1000\permil$), in most pyroxenes and two inclusions (Fig. 2A, Table SI1).

The water contents measured by SIMS in pyroxenes range from below detection limit (~ 4 ppm H_2O) to 387 ppm H_2O. Water contents of pyroxenes from FTIR analyses are about 2 to 10 times lower than those measured by SIMS (Table SI1). This is due to the FTIR providing only minimum values given that the mineral grains could be analyzed only in 2 perpendicular orientations of the infrared polarizer (Table SI2), while a full quantitative estimate requires three (Libowitzky and Rossman, 1996). Sometimes, water contents measured by SIMS can be significantly higher than those measured by FTIR on the same mineral grain if the areas analyzed are not exactly the same. An example is shown in Fig. 3 where the FTIR analyses were performed on the optically clearest areas of a pyroxene from Nakhla (~ 1 ppm H_2O), while the SIMS analyses were performed on areas that contained inclusions/exsolutions (19 and 55 ppm H_2O). Most pyroxenes in all five nakhlites analyzed contain <50 ppm H_2O (Fig. 2A). The highest water content for a pyroxene was measured in a pigeonite from NWA 998 with 387 ppm H_2O. Water contents are heterogeneous in pyroxenes with generally less water near edges compared to interiors (Figs. 4–7). One augite from Nakhla, however, exhibits higher water contents towards its Fe-rich edge (Fig. 3).

Only the mesostasis of Y 000593, MIL 03346 and NWA 6148 could be analyzed and is dominated by glass of plagioclase composition mixed with Fe-Ti oxides. The SIMS analyses are thus of a mix of phases and this results in the bottom of the SIMS craters not being very smooth (Figs. 4C and D, SI4A, SI5). Water contents range from 1133 to 7036 ppm H_2O and the δD from −151 to 132‰ (Fig. 2A).

The inclusion analyzed in a NWA 998 pigeonite grain has a plagioclase composition, a low water content of 26 ppm H_2O and a high δD of 2944‰ (Fig. 5). An inclusion in a Nakhla augite is composed of Fe-rich pyroxene and a K-bearing Si-rich phase, and contains 862 ppm H_2O and has a δD of 364‰ (Fig. SI6). The inclusion from a pyroxene in NWA 6149 has a varied composition dominated by plagioclase with micron sized fayalite, Fe-Ti oxides, phosphate and K-feldspar (Fig. SI4B). The part of the melt inclusion dominated by plagioclase contains 2862 ppm H_2O and has
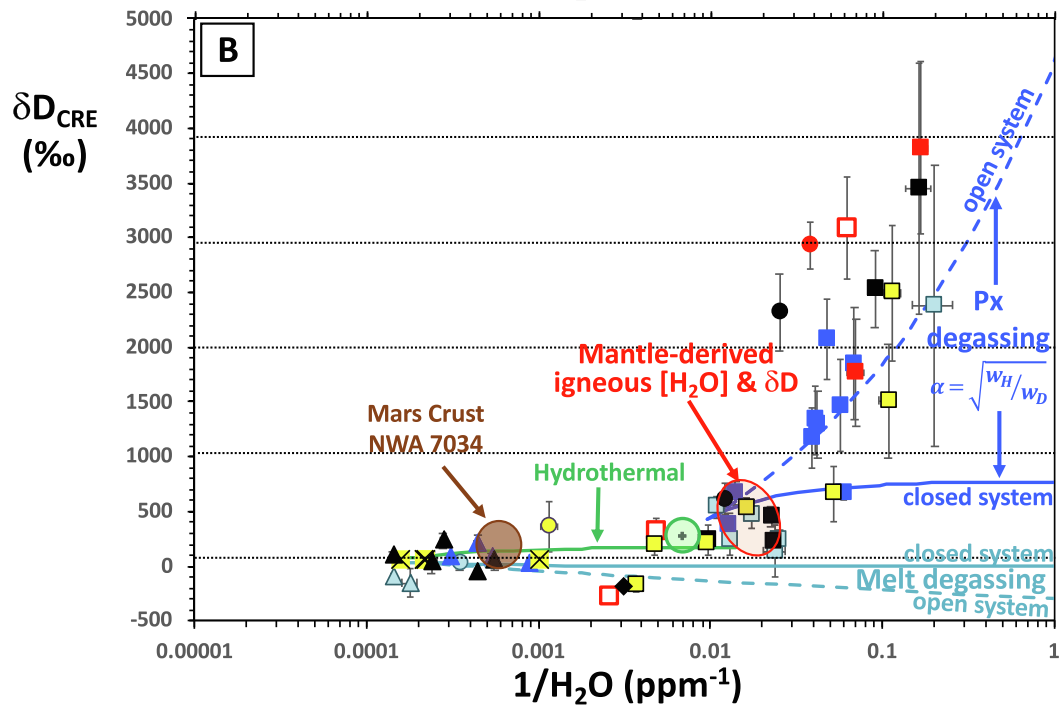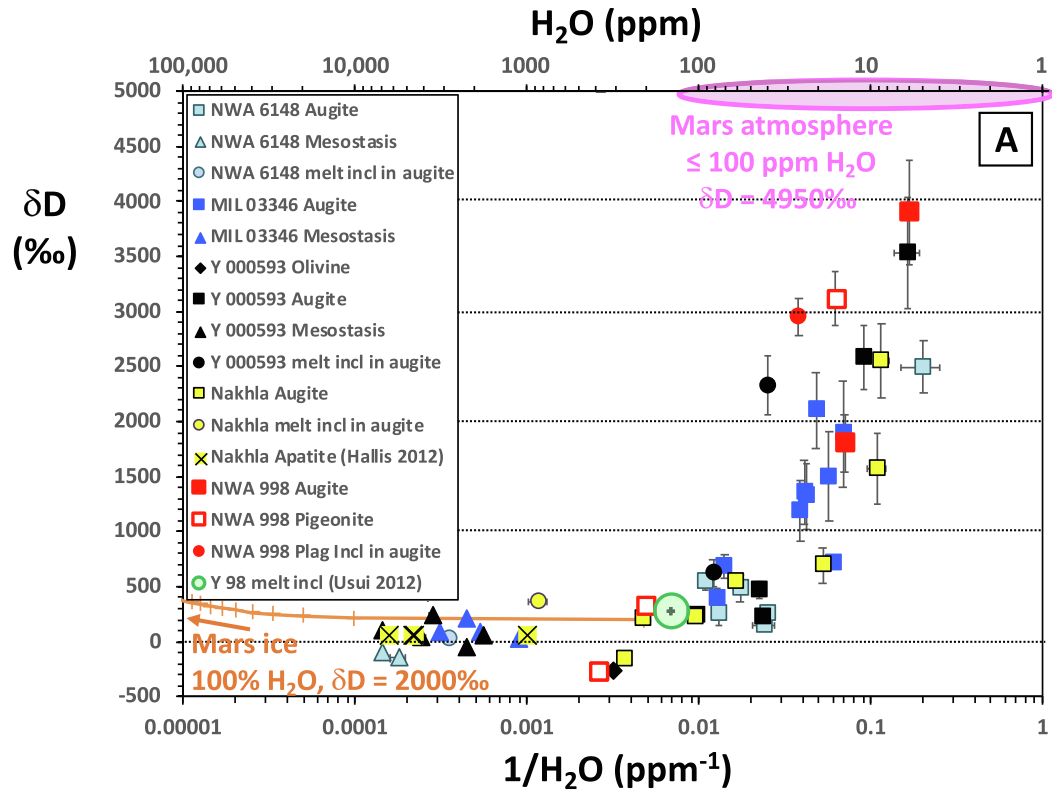
a δD of 22‰. The melt inclusions of Y 000593 are also heterogeneous (Fig. SI3A). Two analyses were performed in one melt inclusion of Fe-rich pyroxene composition (Mg# = 44) and gave different values (Px3 MI B1 and B2 in Fig. SI3A): 40 ppm H_2O and 619‰, and 83 ppm H_2O and 2327‰.

No water was detected in olivines except in those from Y 000593. One Y 000593 olivine contains ~ 320 ppm H_2O and records some of the lowest δD (−268 and −147‰) that we measured (Fig. SI6B), while another with less clinopyroxene inclusions has water content below detection limit for the SIMS. Analyses by FTIR in all these olivines, however, exhibited a wide OH band (Fig. 1C). The discrepancy between the SIMS and FTIR data likely stems from the larger volume analyzed by FTIR which likely included some of the inclusions. Given that the FTIR spectra indicate that the water detected in the Y 000593 olivines is not related to H lattice defects but may be in inclusions, no single absorption coefficient can be applied and no water content can be calculated from these spectra. A SIMS analysis of a Y 000593 olivine results in 320 ppm H_2O and a δD of −268‰ (Fig. SI3B). Nakhla olivines also contain elongate inclusions that could be avoided sometimes but not always during analyses, and yet no water was detected in Nakhla olivines, either by FTIR or SIMS. The olivines of MIL 03346 and NWA 6148 appear clear and those of NWA 998 sometimes have planes of fluid inclusions, and none have detectable levels of water.

3.3. Major and trace element concentrations in pyroxene, olivine and mesostasis

Major and rare-earth element (REE) content variations in nakhlite phases (Fig. SI7, 8 and 9) are similar to previously published data (Bunch and Reid, 1975; Harvey and McSween, 1992; Wadhwa and Crozaz, 1995; Mikouchi et al., 2003; Wadhwa et al., 2004; Imae et al., 2005; Day et al., 2006; Treiman and Irving, 2008; Hallis and Taylor, 2011; Udry et al., 2012; Jambon et al., 2016; Balta et al., 2017; Udry and Day, 2018). The mm-size augites have relatively homogeneous major element composition, save for $\sim 50\ \mu m$ Fe-rich edges (Mg# < 60). Only the augites in NWA 6148 exhibit major element zoning. The augites are characterized by a dome-shaped REE pattern when nor-

Fig. 1. FTIR spectra in the O—H vibration region of nakhlite pyroxene (PX), mesostasis and olivine. Sample thickness is normalized to 1 cm and the spectra vertically off-set for clarity. Abs. = absorbance. For pyroxene and olivine, two spectra per mineral are shown, taken with the infrared polarizer in two perpendicular directions which are aligned parallel (//) to the crystal's indicatrix axes, i.e. // γ and // α or // β. (A) Nakhlite pyroxenes exhibit OH bands only // γ (light blue fields) and at 3620, 3615 and 3450 cm^{-1} (marked with dotted black lines), typical of intrinsic H in pyroxene. The exception is Px7 in NWA 6148 that has a large OH band between 3700 and 3000 cm^{-1} likely due to OH in inclusions (lined light-blue pattern), but also exhibits sharp OH bands at 3670 and 3400 cm^{-1} (Px7 is the augite shown in Fig. 6). (B) Unpolarized spectrum of the mesostasis of NWA 6148. Sharp bands at 3567 and 3400 cm^{-1} may be intrinsic H in olivine (light blue field) while the overall large band (lined light-blue pattern) results of the combination of OH in the various phases of the mesostasis (glass, feldspar, pyroxene, phosphate). (C) No OH bands were detected in nakhlite olivines, except in those of Y 000593 which are characterized by a large OH band between 3000 and 2800 cm^{-1}, symptomatic of water in inclusions (lined light-blue pattern). A band at 3180 cm^{-1} may be caused by intrinsic H (H filled defect in an Mg-vacancy, light blue field). Small bands <3000 cm^{-1} are due to a negligible surface-organics contamination. Also shown in A and C are the FTIR spectra of the pyroxene and olivine used as blanks in the SIMS analyses (grey lines labelled Blank) and that are experimentally-dehydrated diopside and forsterite from a Kilbourne Hole mantle xenolith. No OH bands are detected in the FTIR spectra of the blanks. (For interpretation of the references to colour in this figure legend, the reader is referred to the web version of this article.)

Fig. A: Plot of δD (‰) versus $1/H_2O$ (ppm^{-1}) and H_2O (ppm). Legend: NWA 6148 Augite, NWA 6148 Mesostasis, NWA 6148 melt incl in augite, MIL 03346 Augite, MIL 03346 Mesostasis, Y 000593 Olivine, Y 000593 Augite, Y 000593 Mesostasis, Y 000593 melt incl in augite, Nakhla Augite, Nakhla melt incl in augite, Nakhla Apatite (Hallis 2012), NWA 998 Augite, NWA 998 Pigeonite, NWA 998 Plag Incl in augite, Y 98 melt incl (Usui 2012). Mars atmosphere ≤ 100 ppm H_2O, $\delta D = 4950$‰. Mars ice 100% H_2O, $\delta D = 2000$‰.

Fig. B: Plot of δD_{CRE} (‰) versus $1/H_2O$ (ppm^{-1}). Labels: Mars Crust NWA 7034, Hydrothermal, Mantle-derived igneous [H_2O] & δD, Px degassing, open system, closed system, $\alpha = \sqrt{w_H/w_D}$, Melt degassing, open system, closed system.

malized to CI carbonaceous chondrites (/CI) (Anders and Grevesse, 1989), with Nd at the apex (Fig. SI8A). High field strength elements (HFSE) exhibit negative anomalies relative to the REE/CI (Fig. SI9A). Average trace element patterns of augites/CI are parallel for all five nakhlites for REE, HFSE, B, As, Sr, Y, Sc and V. The augites of NWA 6148 have lower Mg# (∼57) in their interior and higher REE contents compared to the other nakhlites analyzed here. Averages of incompatible trace element contents of augite interiors increase about four times from Nakhla, through Y 000593, MIL 03346 and NWA 998 to NWA 6148 (Fig. SI9A); i.e. the ones with intermediary cooling rates (Nakhla, Y 000593) having the lowest amounts. The augites of Nakhla and Y 000593 also have major element compositions extending to "more primitive" values, recording some of the highest Mg# and lowest Al_2O_3 and CaO contents compared to other nakhlites (Fig. SI7A and B). Positive correlations are evidenced between incompatible trace elements (REE, Y, HFSE, Sc, Ga, V) and Al_2O_3, CaO contents and rough negative correlations with Mg# in augites of each nakhlite (Fig. SI7A and B). At the scale of individual augite grains, however, the Fe-rich edge does not always have higher incompatible trace element contents compared to the interior (for example Ce in Figs. 4, 6 and 7F). A pigeonite grain from NWA 998 has LREE-enriched edges compared to its interior, relative to HREE and when normalized to chondrites (Figs. 5 and SI8C). Some trace elements do not correlate with Mg# or Al_2O_3 in augites, such as Li, B, Tl, Pb, As, Sn.

3.4. Water contents and δD variations with other elements

When the water content of pyroxene is low (<50 ppm H_2O), no correlation between major and trace element and water contents are observed, whether at the scale of one nakhlite or within individual grains (Fig. 7). When a pyroxene grain contains areas with higher water contents, correlations with major element content and analysis location in individual grains start to emerge: at the grain edges, water content decrease (Figs. 4 and 6) or increase (Fig. 3). The D/H ratio sometimes increases towards the edge of a pyroxene grain (Fig. 4) and sometimes decreases (Figs. 3 and 6). In particular, the water content increases while the δD decreases from interior to edge, correlating with major elements (Al_2O_3 increase, Mg# decrease) in one

augite from Nakhla (Figs. 3 and 8). In the mesostasis of Y 000593, water contents correlate with Mg# or MgO/ FeO (Figs. 4 and 9A).

4. INTERPRETATION

4.1. Terrestrial contamination

All nakhlites analyzed here were found either in Antarctica (MIL and Y) or in hot deserts where they were subjected to terrestrial alteration. Given that such alteration occurs via the circulation of fluids in shock-induced fractures, terrestrial alteration is generally considered low for nakhlites which have not been shocked strongly. Terrestrial alteration would be expected to lower the δD (towards and even below 0‰, the δD of the Earth's hydrosphere) and increase the water content of affected phases (Gonfiantini, 1978; Lécuyer et al., 1998; Stephant et al., 2018). The concern is thus that the low δD, high water content end of the trend in Fig. 2 could be, partly, due to terrestrial contamination.

First, we purposefully selected (i) fresh mineral phases devoid of visible alteration; (ii) areas devoid of fractures for SIMS analysis and verified the lack of fracture by SEM imaging of the SIMS craters post-analysis, and (iii) area devoid of grain boundaries in all phases except the mesostasis (Figs. 4B and C, SI4A and SI5) and some melt inclusions (those of Nakhla and NWA 6148; Figs. SI6 and SI3) where analysis of multiple phases could not be avoided. For the mesostasis, the concern is that terrestrial alteration fluids could have seeped at grain boundaries and that our SIMS analyses could have incorporated the water and H isotopic signature of these fluids, and iv) minerals located as far as possible from the edge of the meteorites. Stephant et al. (2018) experimentally demonstrated that desert alteration of the highly fractured martian meteorite Tissint only affected the water content and δD of minerals next to the edge of the meteorite chunk exposed to atmosphere.

Second, REE patterns can be used to detect terrestrial contamination in meteorite phases (Crozaz et al., 2003). A positive Ce anomaly in a chondrite normalized pattern has been suggested to characterize oxidation of meteorite phases during terrestrial alteration of meteorites (Crozaz et al., 2003). However, the pyroxenes (Fig. SI8), olivines

Fig. 2. Deuterium to hydrogen ratios expressed in δD (‰) versus the reciprocal of the water content ($1/H_2O$) obtained by SIMS on nakhlite pyroxene (squares), inclusions in pyroxenes (incl, circles), and mesostasis (triangles). (A) Blank-corrected water content and δD, and reservoirs or processes that cannot explain the data. (B) δD corrected for cosmic ray exposure spallation effects ($δD_{CRE}$) using Merlivat (1976) H and D production rates, and reservoirs and processes that are involved in producing the range of data. Data for a melt inclusion from olivine-phyric depleted shergottite Y 980459 (Y98 melt incl) is included for reference as it has so far been taken as being the closest we have to Mars mantle values (Usui et al., 2012). Similarly, data for the breccia NWA 7043 is shown to represent martian crustal composition (Agee et al., 2013). The orange line with tick marks in A is a mixing model between igneous martian water contents and δD and those of martian ice (Usui et al., 2015). The tick marks represent 1% increments of mixing. Simple mixing with ice cannot reproduce the pyroxene data. In B, the bright blue lines show degassing models of H and D loss from already crystallized pyroxene, and the lighter blue lines show degassing models of water (OH and H_2O) loss from a melt. The green line shows the evolution of δD during interaction of a melt with hydrothermal fluids at 700 °C. The pyroxene degassing model is the closest to the data for the water-poor pyroxenes. The low δD of the evolved phases can be explained by a combination of degassing of the intercumulus melt and interaction with hydrothermal fluids. The red ellipse encompasses water contents and δD that are thought to be igneous, i.e. derived from the nakhlite mantle source. (For interpretation of the references to colour in this figure legend, the reader is referred to the web version of this article.)

and mesostasis (Fig. SI10) analyzed here do not exhibit Ce anomalies. The LREE can also be affected by terrestrial alteration in low-Ca pyroxene (Crozaz et al., 2003) and it may explain the higher LREE relative to HREE at the edge (La/Yb = 9.6) of the NWA 998 pigeonite grain relative to its center (La/Yb = 1.2; Fig. SI7C). The olivines analyzed here all have depletions in LREE relative to HREE, inconsistent with terrestrial alteration (Fig. SI10).

Third, the water content of the mesostasis (1100–7850 ppm H_2O), which is dominated by plagioclase, is
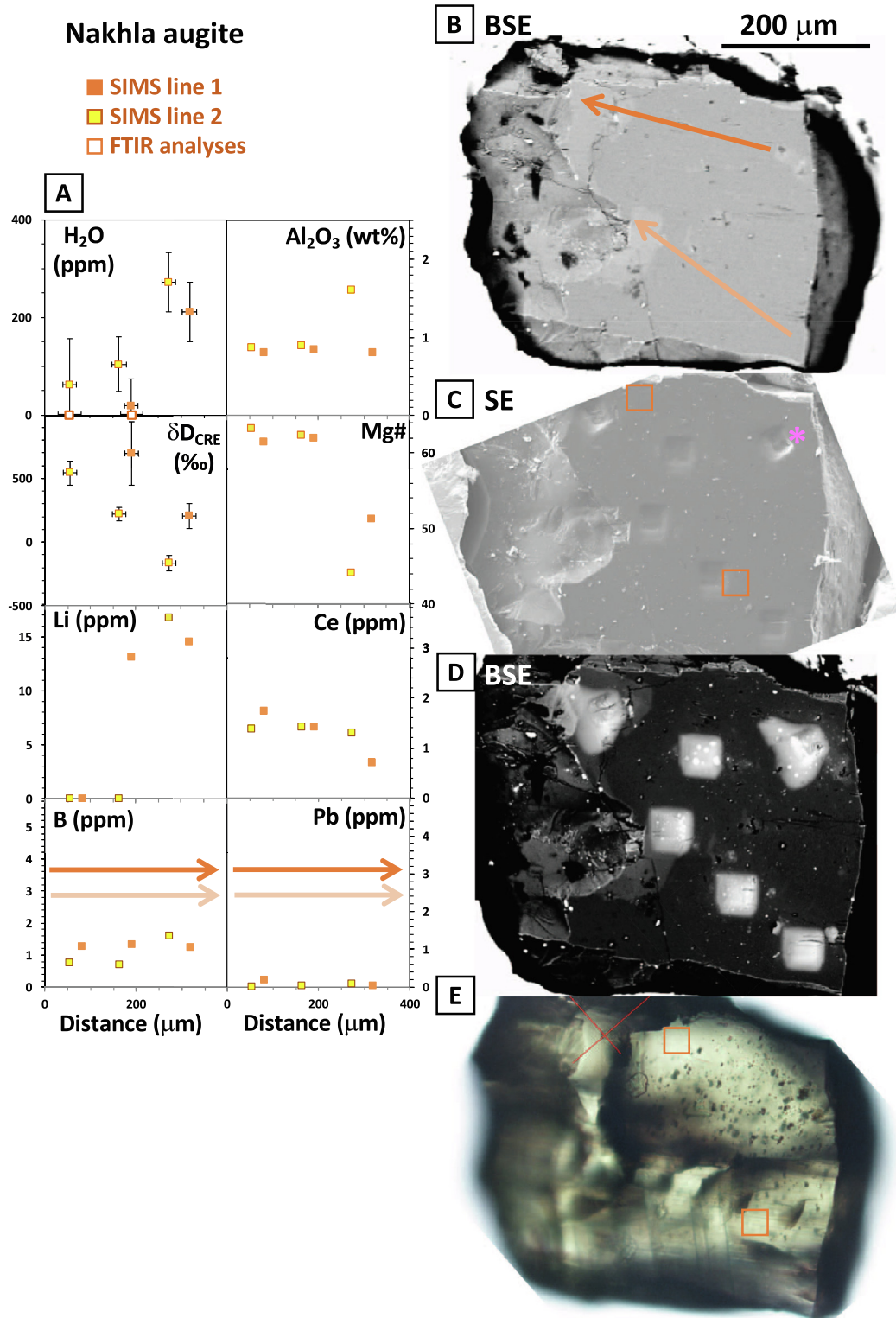
higher than that of most terrestrial igneous plagioclases (<1000 ppm H_2O; Johnson and Rossman, 2004). However, this does not necessarily imply that terrestrial alteration is responsible for the high water contents. When water is located in fluid inclusions instead of lattice defects, water contents ~2000 ppm H_2O are common in terrestrial plagioclases (Johnson and Rossman, 2004). Moreover, we analyzed multiple phases in the mesostasis that can include water-rich late crystallized phases such as evolved glasses and apatite, which contributions could have enhanced the water content of the mesostasis analyses. Finally, a positive correlation of water content and MgO/FeO ratio in the mesostasis of Y 000593 can be best explained by igneous rather than terrestrial alteration processes (Figs. 4 and 9A, see Section 4.4.1.1).

In summary, although terrestrial contamination cannot be completely ruled out for some of the mesostasis and melt inclusion analyses, we consider their water content and δD to be the results of processes on Mars. The ranges of water and REE contents and δD of the nakhlite pyroxenes and olivines are thus not considered to have resulted from terrestrial alteration.

4.2. Processes potentially affecting H during meteorite transit from Mars to Earth

Addition of H by solar wind to the surface of airless extraterrestrial bodies is limited to <200 nm depths (Keller and McKay, 1997; Hashizume et al., 2000; Chamberlin et al., 2008; Burke et al., 2011; Bradley et al., 2014). This and the fact that the exterior of meteorites ablate during their passage through the Earth's atmosphere rules out H implantation by solar wind as a contribution to our measured water contents.

Exposure to cosmic rays, on the other hand, results in spallation processes that produce H and D to several meters depths in meteoroids, with D/H produced in higher ratios than SMOW (Reedy, 1981; Reedy et al., 1983; Eugster et al., 2006). However, the time of exposure of the nakhlites to cosmic rays (~11 My; Terribilini et al., 2000; Eugster et al., 2002; Christen et al., 2005; Korochantseva et al., 2011) is too short to significantly alter the H and D contents of nakhlite phases, as detailed in SI3 and Table SI4. The difference between the spallation corrected δD (δD$_{CRE}$, calculated using H and D production rates of (Merlivat, 1976) and the uncorrected δD are minor relative to the range of δD exhibited by the nakhlite phases to the point of being barely visible when comparing Fig. 2A and B: larger corrections occur at low water contents (<100 ppm H_2O, δD on

average 43‰ lower and with larger error bars) and are smallest at high water contents (>100 ppm H_2O, δD on average 0.3‰ lower). The water contents hardly changed, i.e. they are similar within uncertainties (Table SI1). The range of δD observed in nakhlite pyroxene (>4000‰, Fig. 2) cannot be explained by cosmic ray interactions.

4.3. Interaction with surficial martian reservoirs

The atmosphere of Mars has an elevated D/H ratio that results from preferential loss of H to space throughout its history (Yung et al., 1988; Chassefière and Leblanc, 2004; Webster et al., 2013). During this process, fractionation of the isotopes of hydrogen result in an atmosphere with an average δD of 4950‰ (Owen et al., 1988; Webster et al., 2013). Surficial reservoirs (crust, ice, alteration products) are thus expected to have an elevated δD (>500‰) inherited from interaction with the atmosphere (e.g., Watson et al., 1994; Boctor et al., 2003). Here, we assess whether the high δD (500–4500‰) of the martian pyroxenes and some melt inclusions (Fig. 2) could have been influenced by interaction with surficial martian reservoirs. Two possible scenarios are examined: (1) shock implantation, and (2) interaction with surficial fluids.

4.3.1. Shock
The high pressure, albeit for a brief time period (≤1 s), and potentially high temperature, that characterizes shock (e.g, Sharp and DeCarli, 2006) could potentially increase H mobility in martian rocks and their minerals during an impact event. However, as detailed in SI4, shock is unlikely the cause of the high δD and low water contents of most nakhlite pyroxenes because: (i) nakhlites are minimally shocked (Fritz et al., 2005a,b), (ii) Xe isotope systematics shows that shock implantation of volatiles is limited to grain boundaries in nakhlites (Gilmour et al., 2001); (iii) shock experiments on hydrous phases resulted in increases of δD that are small compared to the δD range observed in nakhlite phases (Tyburczy and Ahrens, 1988; Tyburczy et al., 1990; Minitti et al., 2008a,b; Sekine et al., 2012, 2015).

4.3.2. Interaction with surficial fluids
4.3.2.1. Interaction with atmosphere and ice. The next hypothesis to test is that the pyroxenes had initially low "mantle" δD (<500‰) and that interaction with surficial fluids increased their δD. Although the martian atmosphere contains little water vapor at present (<150 ppm H_2O; Rodin et al., 1997; Fedorova et al., 2009), equilibration of

Fig. 3. Water content, δD, Al_2O_3, Ce, Pb, Li and B contents, and Mg# (Mg/(Mg + ΣFe^{2+})) along cross sections through a zoned augite from Nakhla. The δD values are corrected for cosmic ray exposure (δD$_{CRE}$). The error bar on the distance in panels featuring water content and δD are ±15 μm (i.e. correspond to a diameter of ~30 μm for the area analyzed by SIMS). The Mg# profile and the lighter grey at the edge of the pyroxenes compared to its interior in the back-scattered electron (BSE) image (B) indicates lower Fe contents. Panels C and D show secondary electron (SE) and BSE images of the SIMS craters. Panel E shows a plane-polarized photo of the augite and the squares indicate where FTIR analyses were performed, i.e. on the locations having the clearest path (minimum amount of inclusions) through the mineral for the infrared beam. The pink star is next to a SIMS crater that had a hole at its bottom and which analysis was not taken into account in the interpretation. This Nakhla augite preserved evidence for water content and δD variations being controlled by pyroxene igneous crystallization. (For interpretation of the references to colour in this figure legend, the reader is referred to the web version of this article.)

Y 000593 augite and mesostasis
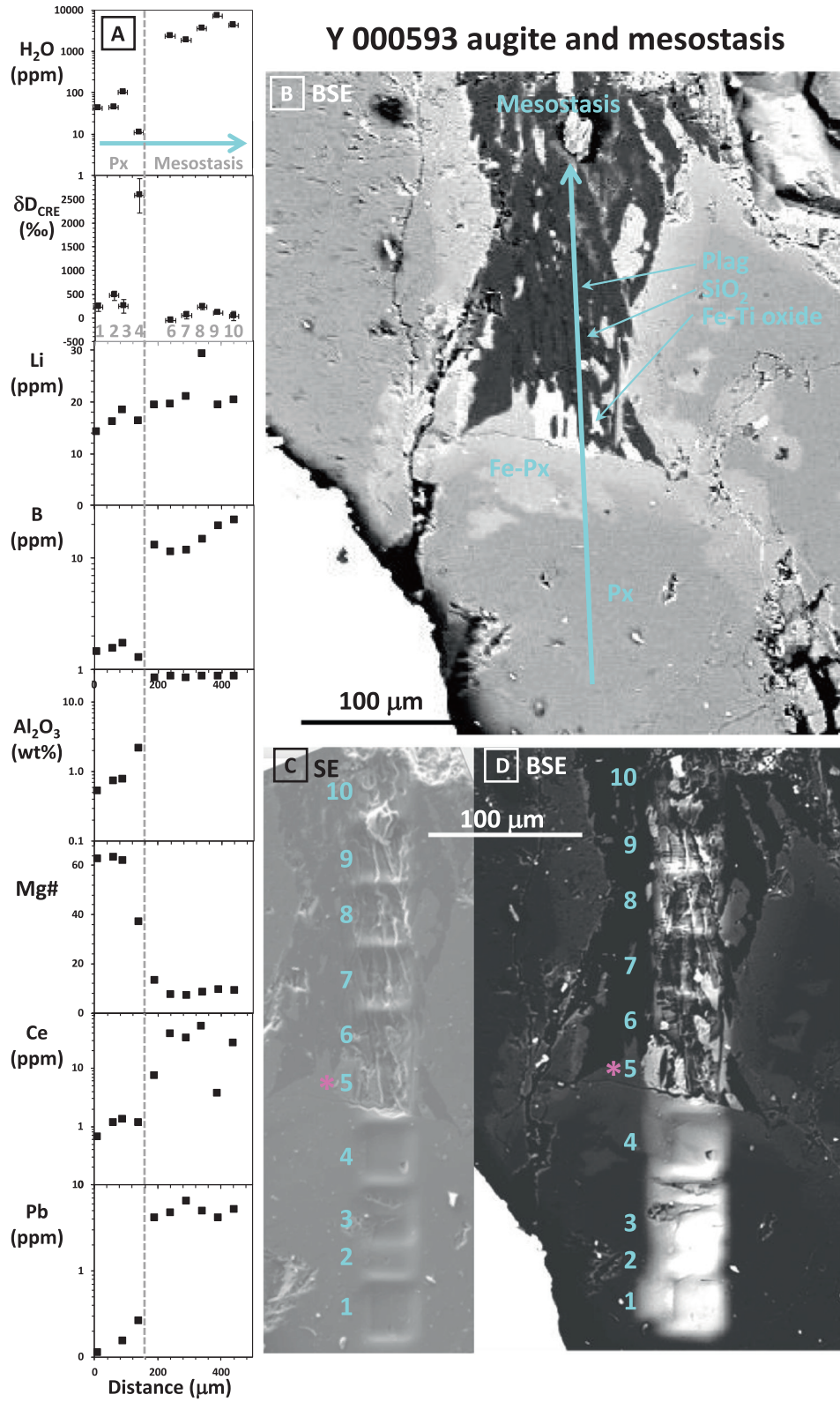
the pyroxenes with this 'dry' atmosphere at martian surface temperatures is unlikely. First, only the pyroxene grains directly exposed to the atmosphere, such as at the surface of a lava flow, would be affected. Second, the nakhlite crystallized during the Amazonian (Nyquist et al., 2001; Cohen et al., 2017), a time when the climate of Mars was likely so dry that, since then, rain was unlikely and aqueous alteration was rare (Carr and Head, 2010). Third, diffusion rates of H and D in pyroxene would be too slow to significantly change the pyroxene water content. The pleochroism and position of the OH bands in the FTIR spectra of the Nakhlite pyroxenes (Fig. 1) shows that the water analyzed is located in the mineral lattice, and not in water-rich inclusions (except for NWA 6148 Px7). The diffusion of H incorporated in that manner in pyroxene can be modelled (details in SI6) with experimentally determined diffusion rates (Hercule and Ingrin, 1999). At the average temperature of the martian surface determined from Viking landers and rover measurements; (-43 °C; Seiff and Kirk, 1977; Fergason et al., 2006), however, this modeling shows that only the outer 0.06 µm of a pyroxene grain would be affected after 1.3 Ga, the crystallization age of the nakhlites (dotted blue line in Fig. 10).

Another possibility is that the outcrop from which the nakhlites originate has been covered by ice that could either be the seasonal water ice at the poles, local condensate (Webster et al., 2013), or underground ice (Farmer et al., 1976; Bibring et al., 2004; Mouginot et al., 2012; Orosei et al., 2015). The isotopic H ratio of martian ice has never been measured in situ, but an estimate of a δD of 1000–2000‰ comes from modelling shergottite impact-melt data (Usui et al., 2015). Hydrogen exchange with surficial ice could increase the δD of the martian phases and is modelled with a simple binary mixing (orange line in Fig. 2A). However, this process would also increase the amount of water in the nakhlites, the opposite of what the analyses shows. Changing the δD of ice to higher (+5000‰) or lower values (e.g., 0‰) does not provide a better fit to that observed in the nakhlite pyroxenes.

4.3.2.2. Interaction with hydrothermal fluids 4.3.2.2.1. Mesostasis. A more realistic scenario is infiltration of martian surficial hydrothermal fluids through the nakhlite cumulate pile at temperature >25 °C (Bridges et al., 2001; Filiberto et al., 2014; Liu et al., 2016). Nakhlites show evidence of low temperature (≤150 °C) hydrothermal activity on Mars with the

circulation of brines perhaps linked to an impact occurring nearby the nakhlite pile (Gooding et al., 1991; Bridges and Grady, 2000; Bridges et al., 2001; Treiman and Irving, 2008; Changela and Bridges, 2010; Hallis and Taylor, 2011; Bridges and Schwenzer, 2012; Cartwright et al., 2013; Lee et al., 2013; Hallis et al., 2014; Niles et al., 2017). Alteration features are typically localized in veins, leaving most of the igneous textures and minerals intact. A martian alteration fluid may have elevated δD reflecting exchange with the atmosphere or ice. Analysis of smectites in Nakhla suggest that a δD of 1165 ± 116‰ is a minimum value for martian aqueous surface fluids (Hallis et al., 2012b). Other estimations for the δD of martian alteration fluids range from 500–870‰ (Liu et al., 2016), 1000–2100‰ (Usui et al., 2015) to 4000‰ (Leshin et al., 2013). The δD of martian surficial fluids are higher than those of the nakhlites' mesostasis (-151 to 231‰), suggesting that this mesostasis was unaffected by martian surficial aqueous fluids.

On the other hand, the nakhlite mesostasis δD are similar to that of bulk measurements of the one martian crustal breccia known, NWA 7034: step heating of bulk aliquots of this meteorite yielded δD from -100 to +327‰ (Agee et al., 2013). The low δD of NWA 7034 water released at 50 °C likely originated, at least in part, from terrestrial alteration since δD ~ 0 have been measured in situ in Fe-oxyhydroxides as alteration products of martian pyrite (Lorand et al., 2015). The high δD water released at 900 °C may be intrinsic to the breccia, which has high water content of $\sim$0.6% (Agee et al., 2013). Incorporation of crustal material, perhaps via interaction with deep crustal fluids (as opposed to surficial fluids with higher δD), or via melting/assimilation at the edge of a magma chamber, is thus a more likely explanation for the δD of the nakhlite mesostasis. This scenario of hydrothermal fluids mixing with the intercumulus melt is supported by evidence that the magmatic hydrous phases of nakhlites (apatite, amphibole) crystallized from a melt that was Cl-rich (McCubbin et al., 2013; Filiberto et al., 2014; Giesting and Filiberto, 2016). Although it has been suggested that this high amount of Cl could be igneous, i.e. the melt's mantle source was Cl-rich (Filiberto and Treiman, 2009), it is most likely exogenous. Chlorine was added to the melt at crustal levels via mixing with Cl-rich hydrothermal fluids and brines circulating through the nakhlite melt prior to complete crystallization at the martian surface or in a sill (Cartwright et al., 2013; McCubbin et al., 2013; Magna et al., 2015;

◄

Fig. 4. Water content, δD, Li, B, Al_2O_3, Ce and Pb contents and Mg# (Mg/(Mg + ΣFe^{2+})) along cross sections through a zoned augite and mesostasis of Y 000953. The δD values are corrected for cosmic ray exposure (δD_{CRE}). The Mg# profile (A) and the lighter grey at the edge of the Y 000593 augite (Px) compared to its interior in the back-scattered electron (BSE) image (B) indicates lower Fe contents (Fe-Px). The error bar on the distance in the H_2O and δD panels are ± 15 µm (i.e. correspond to a diameter of $\sim$30 µm for the area analyzed by SIMS). C shows a secondary electron (SE) image and D shows a BSE image of the SIMS craters, with 1–10 numbers to better identify the location of the analyses shown in (A). The pink star is next to a SIMS crater that has obvious fractures and which SIMS analysis was not taken into account in the interpretation. The bottom of the craters in the mesostasis of Y 000593 are also not smooth which is the result of the mesostasis being composed of multiple phases: mainly plagioclase (Plag.), but also SiO_2 and Fe-Ti oxides. Except the crater right at the boundary between the pyroxene and mesostasis that is clearly on a fracture, the δD of the mesostasis analyses (>-56‰, A) are significantly above that of the SIMS background (-300 to -100‰), and can likely be trusted. The high δD and low water content at the edge of the pyroxenes are consistent with degassing of H and D through an already crystallized pyroxene. (For interpretation of the references to colour in this figure legend, the reader is referred to the web version of this article.)
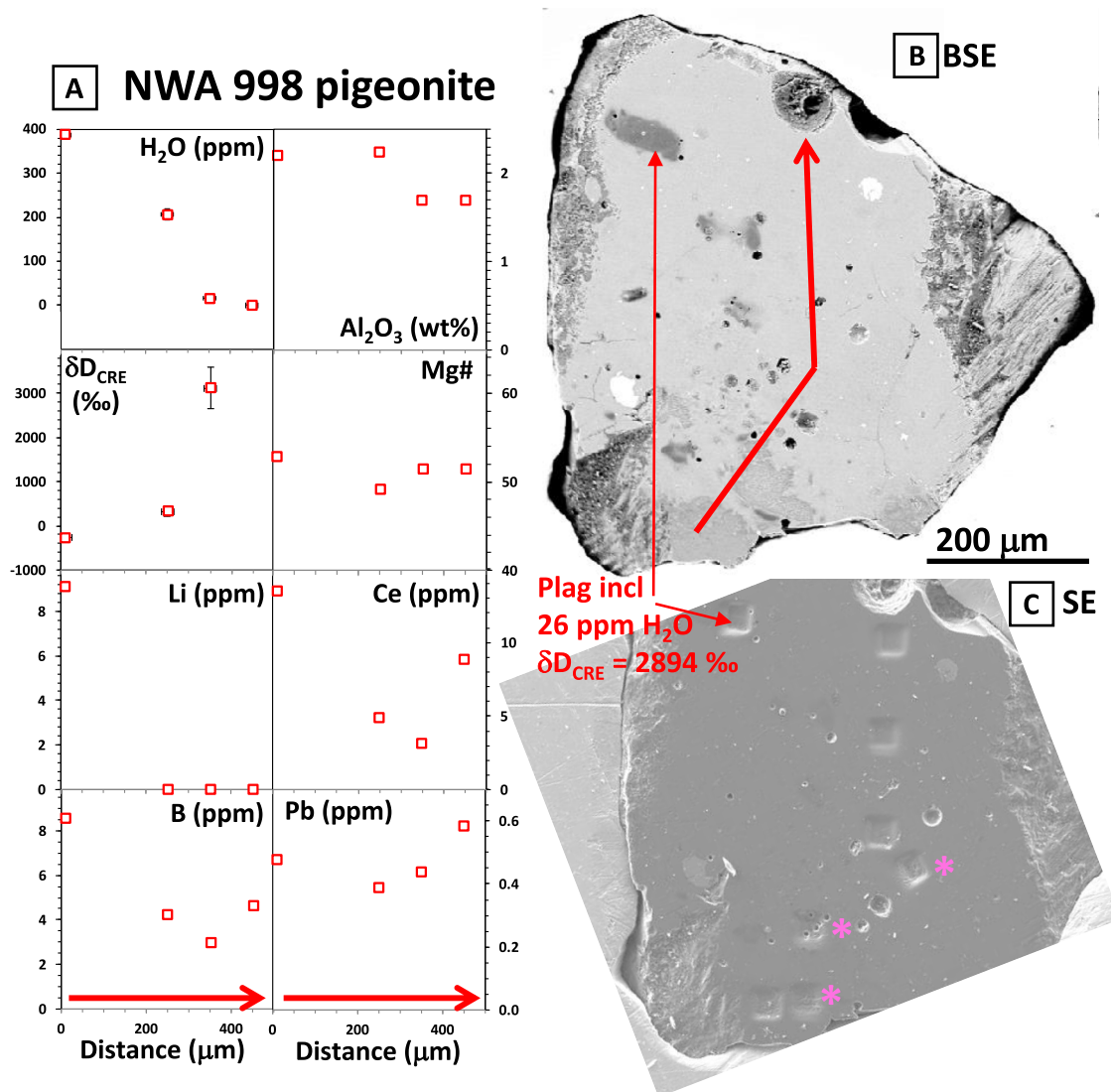
Fig. 5. Water content, δD, Al_2O_3, Li, B, Ce and Pb contents and Mg# $(Mg/(Mg + \Sigma Fe^{2+}))$ along a cross section through a pigeonite from NWA 998. Three of the Li contents and one water content are below detection limits in the NWA 998 pigeonite and are plotted at 0 ppm. Consequently, the one water content below detection limit has no corresponding δD. The δD values are corrected for cosmic ray exposure ($δD_{CRE}$). The error bar on the distance in the H_2O and δD panels are ±15 μm (i.e. correspond to a diameter of ~30 μm for the area analyzed by SIMS). Panel C shows a secondary electron image (SE) of the SIMS craters. The pink stars are next to SIMS craters that have fractures or holes and which analyses were not taken into account in the interpretation. The high δD and low water content at the top edge of the pyroxene are consistent with degassing of H and D through an already crystallized pyroxene. (For interpretation of the references to colour in this figure legend, the reader is referred to the web version of this article.)

Shearer et al., 2018). For example, the range of Cl-F compositions of apatites from the mesostasis in nakhlites, along with their water-poor characteristics, reflect a history of crystallization from a Cl-rich degassing melt (McCubbin et al., 2013). Sulfur isotopes also reveal assimilation of martian salts in the mesostasis, i.e. in the intercumulus liquid when the partially-crystallized nakhlite magma may have flowed on the martian surface (Franz et al., 2014; Dottin et al., 2018).

Fractionation of H isotopes during fluid-melt interaction can be modeled using the equation of De Hoog et al. (2009) to model fluid-melt interaction during melt degassing

(Eq. (SI4)) and the equation of Suzuoki and Epstein (1976, Eq. (SI6)) to calculate the fractionation factor (see details in SI5). There is no fractionation factor available for martian fluid and melt compositions, but experimental studies for aqueous fluids coexisting with aluminosilicate melts are available (Mysen, 2013; Dalou et al., 2015). The results of D/H fractionation using Eq. (SI6) with $a = -126$ and $b = 263$ (Dalou et al., 2015) results in a fractionation factor $\alpha_{fluid-melt}$ of 0.88 at 700 °C, a reasonable temperature for the cooling nakhlite mesostasis melt (Richter et al., 2016). Assuming that the most water-rich mesostasis (Y 000593A with 7036 ppm H_2O and a δD of 104‰) as initial
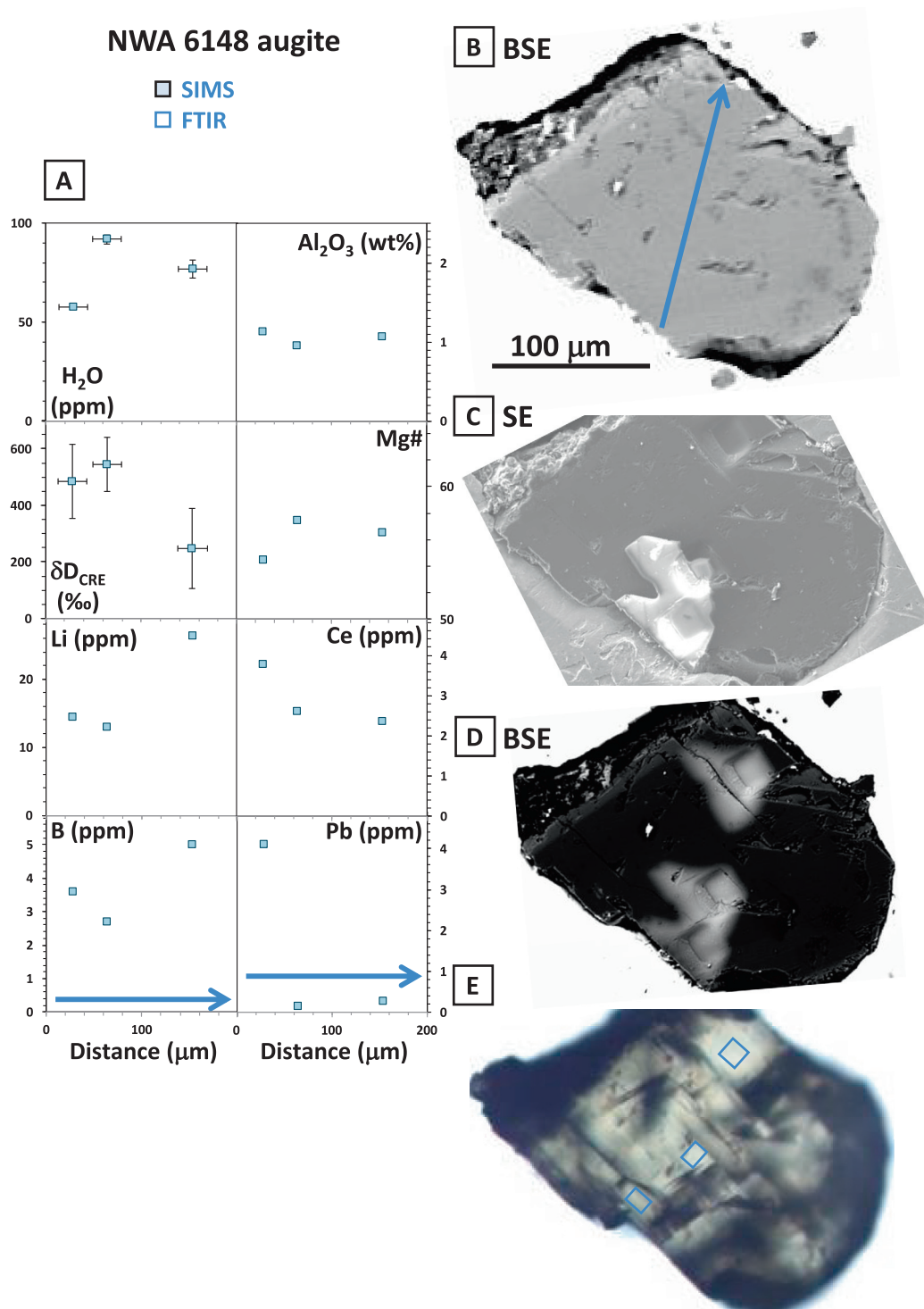
Fig. 6. Water content, δD, Al_2O_3, Ce, Pb, Li and B contents, and Mg# (Mg/(Mg + ΣFe^{2+})) are shown along a cross section through an augite from NWA 6148. The δD values are corrected for cosmic ray exposure (δD_{CRE}). The error bar on the distance in panels featuring water content and δD are $\pm 15\ \mu m$ (i.e. correspond to a diameter of ~30 μm for the area analyzed by SIMS). Panels C and D show secondary electron (SE) and BSE images of the SIMS craters. Panels E shows a plane-polarized photo of the augite and the squares indicate where FTIR analyses were performed, i.e. on the locations having the clearest path (minimum amount of inclusions) though the mineral for the infrared beam. The edges of the augite have lower water content and lower δD than the center, correlating with major element contents, that indicates crystallization from a degassing melt.
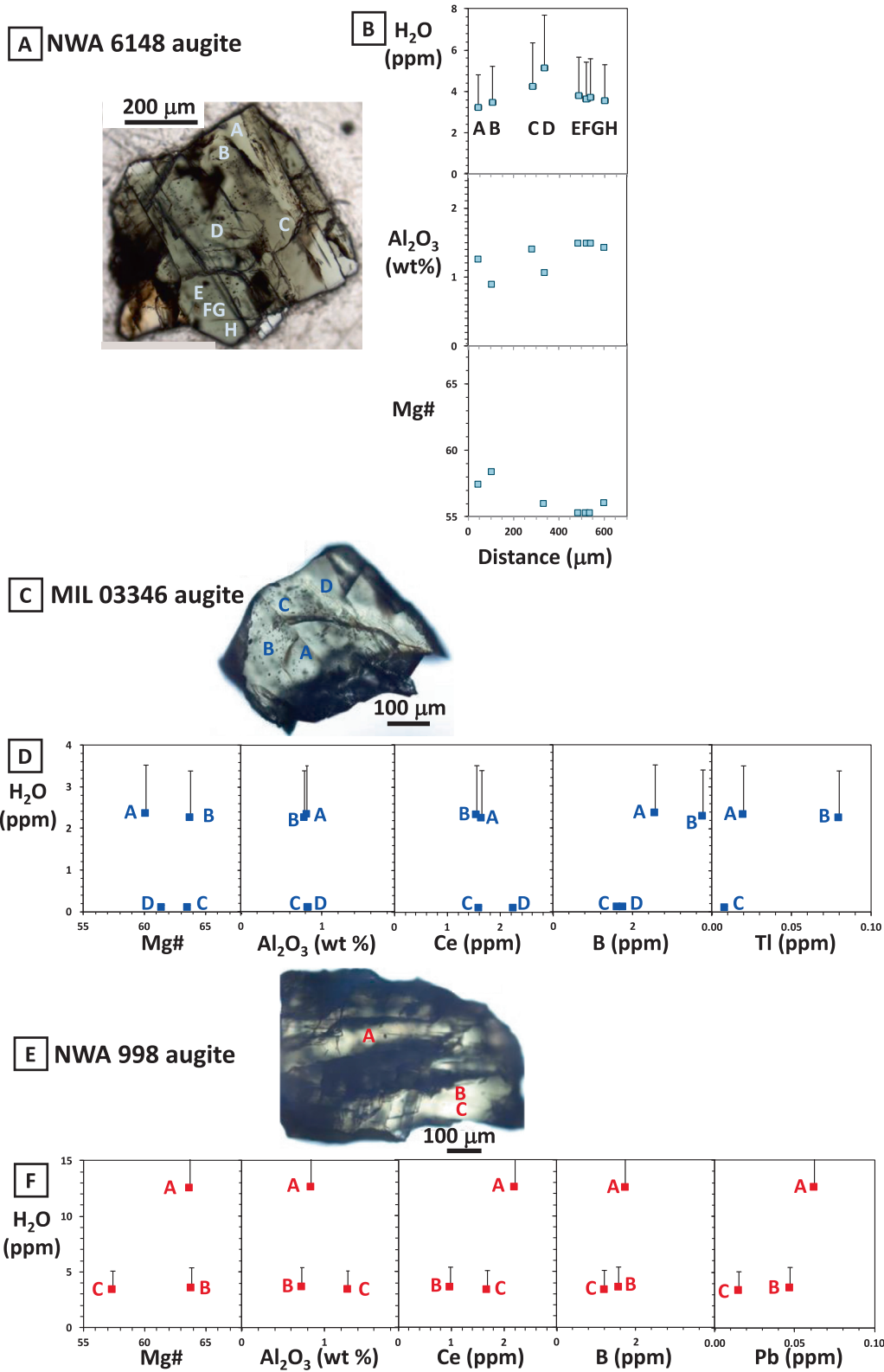
Fig. 7. Water content determined by FTIR, Mg# (Mg/(Mg + Fe)) and Al_2O_3, Ce, B and Tl or Pb contents in augites from NWA 6148 (A and B), MIL 03346 (C and D) and NWA 998 (E and F). Transmission light photos of the pyroxene grains are provided to show the location of each analysis. The lack of correlation between water and major element contents, while pyroxene edges typically have less water than their cores, evidences H degassing from pyroxenes. No water was detected at C and D in the augite from MIL 03346 and the water content is plotted here for illustration at 0.1 ppm H_2O, an arbitrary value below detection limit. Positive error bars of 50% on the water contents indicate that FTIR water contents are minimum values (see SI2.2 for details).
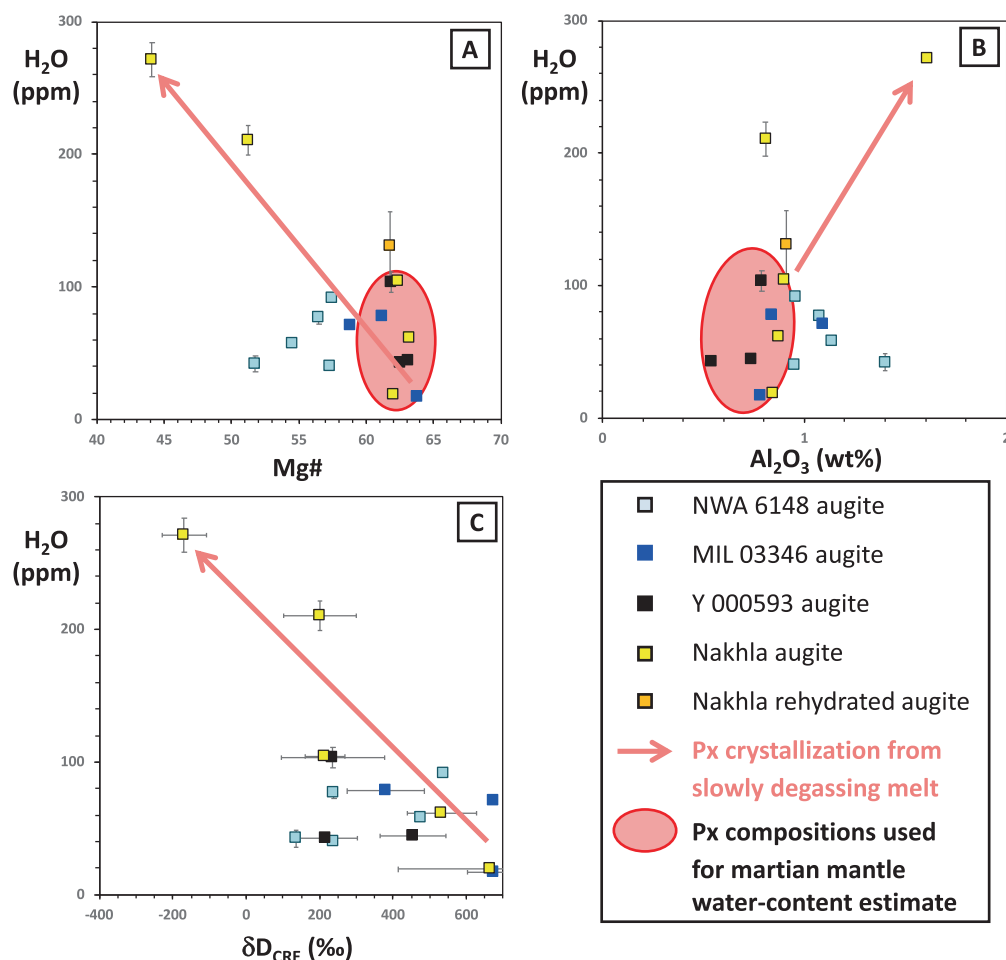
Fig. 8. Water content versus Mg#, Al_2O_3 content in weight % and δD in ‰ in the least degassed nakhlite pyroxenes (>5 ppm H_2O, δD < 700‰). The δD values are corrected for cosmic ray exposure ($δD_{CRE}$). "Nakhla Rehyd. Augite" is an average of analyses of three Nakhla augites that initially contained <10 ppm H_2O and that were rehydrated experimentally at 700 °C and 2 kb by Weis et al. (2017). The red arrow shows the general trend of crystallization during slow degassing exhibited by the Nakhla augite data. The red ellipse encompasses the undegassed Mg-rich augites used to calculate the water content and δD of the martian mantle. (For interpretation of the references to colour in this figure legend, the reader is referred to the web version of this article.)

composition, the resulting modelled δD overlap with the highest δD measured in the mesostasis (green curves in Fig. 11B). If a lower initial δD is chosen (such as that of the mesostasis in NWA 6148 with δD ∼ −95 to −150‰), the fluid-melt δD fractionation curves would pass through most of the δD measured in the mesostasis. Exchange of hydrothermal fluids with the intercumulus melt is thus consistent with the range of δD observed for the mesostasis (Fig. 11B).

4.3.2.2.2. Pyroxene. Theoretically, interaction of the pyroxenes with hydrothermal fluids could either occur before complete crystallization of the nakhlites via the mixing of the hydrothermal fluids with the residual melts and diffusion of H at high temperature into the pyroxenes, or after nakhlite complete crystallization with the fluids seeping along pyroxene grain boundaries at low temperatures.

For the latter case, however, diffusion of H and D is extremely slow through pyroxene and olivine at the low temperatures (<150 °C) under which this hydrothermal

alteration occurred (Bridges and Schwenzer, 2012; Hallis et al., 2014). It has been suggested that hydrothermal fluid temperatures could have reached 700 °C (Filiberto et al., 2014). Typical hydrothermal systems on Earth, however, rarely reach temperatures >300 °C (e.g., Chiodini et al., 2001; Lowell and Rona, 2002). Rather than the ingress of hydrothermal fluids, the 700 °C temperature recorded by scapolite in an olivine melt inclusion from Nakhla (Filiberto et al., 2014) could testify to the evolution of a magmatic volatile-rich melt as a closed system during the cooling of Nakhla. This has been evidenced in a melt inclusion from a MIL 03346 pyroxene (McCubbin et al., 2009). Moreover, as pointed out by Richter et al. (2016), the similarity of Ar ages for all nakhlites (Park et al., 2009; Cohen et al., 2017), precludes heating events above the Ar closure temperature (350 °C) from having occurred after complete crystallization. In other words, temperatures >150 °C for hydrothermal activity in nakhlites are unlikely.
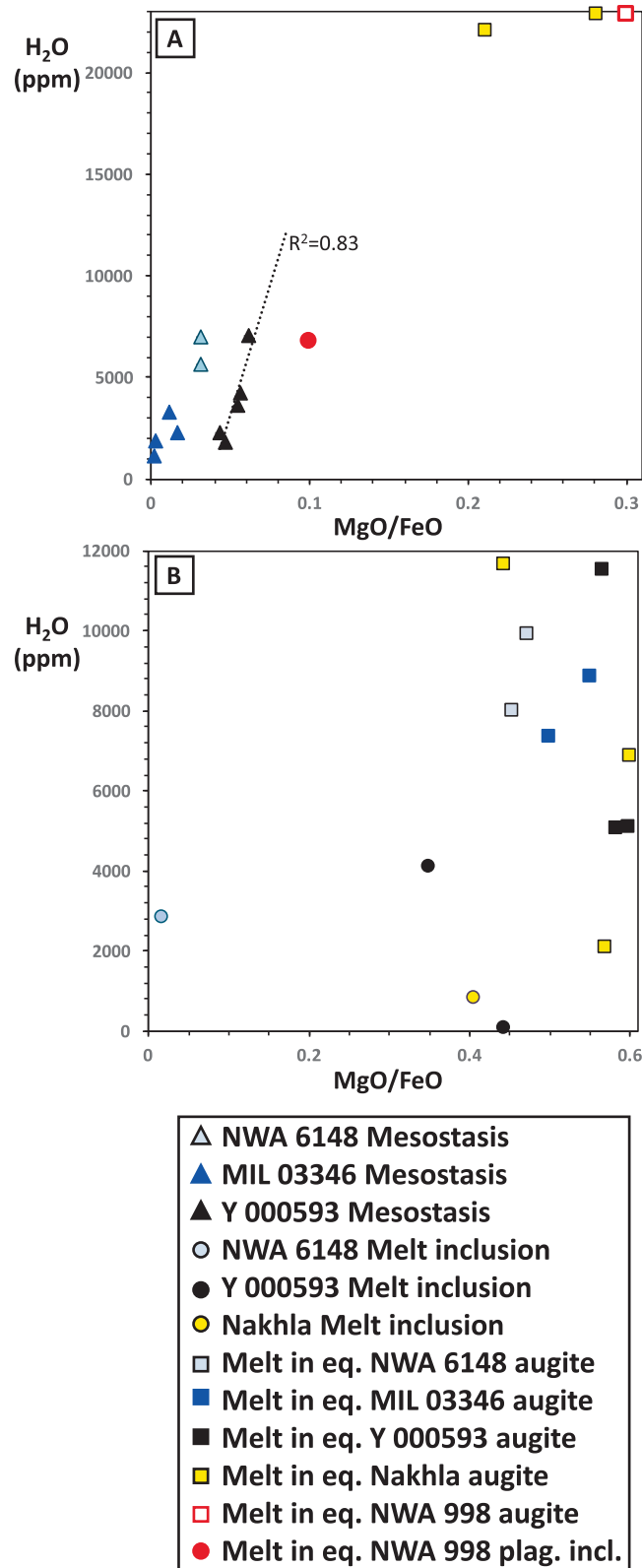
Fig. 9. The water content and MgO/FeO ratio of the mesostasis (A) or of melt inclusions found in pyroxenes (B) compared to those of melts in equilibrium with pyroxenes in nakhlites. (A) Later crystallized least-degassed phases (comparison of mesostasis with Fe-rich augite edges and pigeonite). (B) Earliest crystallized least-degassed phases (comparison of melt inclusions with core of Mg-rich augites). The lower water contents of the inclusions and mesostasis compared to those of melt in equilibrium with pyroxenes is the result of degassing processes. plag. incl. = plagioclase inclusion in the NWA 998 pigeonite of Fig. 5.

The duration of the fluid hydrothermal event(s) that affected the nakhlites is unknown but is likely short enough that H diffusion in olivine and pyroxene was negligible. It could occur during an impact event when ice would melt locally or during volcanic activity. Aqueous alteration resulting from impact in a low permeability media (like a pyroxenite flow) has been modeled to have persisted for a few thousand years (Barnhart et al., 2010). Modeling H diffusion into a pyroxene at 50 °C using a diffusing time of 5000 years adds water only to the 10 μm edge of a pyroxene containing 60 ppm H_2O (SI6, dotted grey curve in Fig. 10). Only if the fluid would come in direct contact with a pyroxene grain continuously for >5 Ma, could it start modifying the water content of the 100 μm edge of the grain (black curve in Fig. 10). At 150 °C, it would take 500 years of continuous exposure to hydrothermal fluids to achieve the same water enrichment of the outer 100 μm of the pyroxene (orange curve in Fig. 10). Continuous exposure for these time spans is, however, unlikely and short duration sporadic episodes are more realistic. In summary, it is unlikely that low-temperature hydrothermal alteration played a significant role in establishing the range of water contents and H isotopes observed in the nakhlite augites.

Hydrogen diffusion into pyroxene and olivine is considerably faster if temperatures are higher, such as igneous temperature when the intercumulus liquid was in contact with the already crystallized pyroxene. Cooling rate estimations for nakhlites suggest that a temperature of <700 °C is reasonable for the cooling intercumulus melt (Richter et al., 2016). At 700 °C, the water content of a mm-size pyroxene containing initially 60 ppm H_2O in continuous contact with a melt containing 3640 ppm H_2O (average of the mesostasis water contents) can be modeled using Eq. (SI10) to have its water content increased 10 times in less than a day within 1 mm of its edge (red curve in Fig. 10). Although the nakhlites are thought to have cooled very rapidly, time estimates for cooling are still of several days (Richter et al., 2016). However, at the time of cooling of the inter-cumulus magma, processes other than simple diffusion of water into pyroxene were at play, such as continuous growth of the augites via crystallization (resulting in the Fe-rich edges; Richter et al., 2016) and degassing (resulting in H loss from
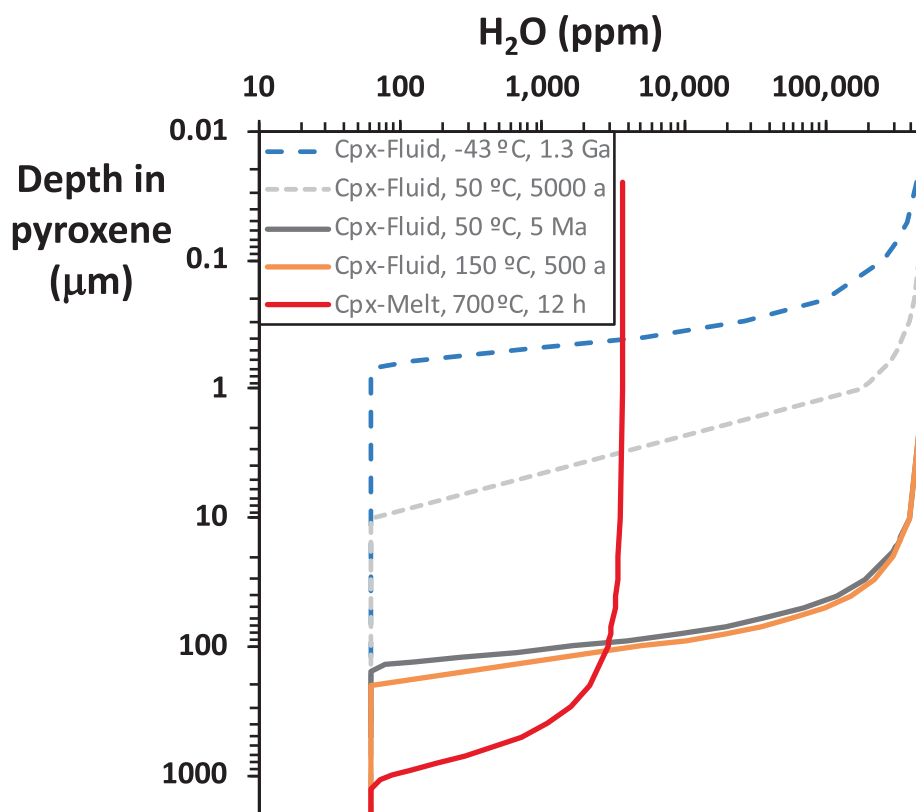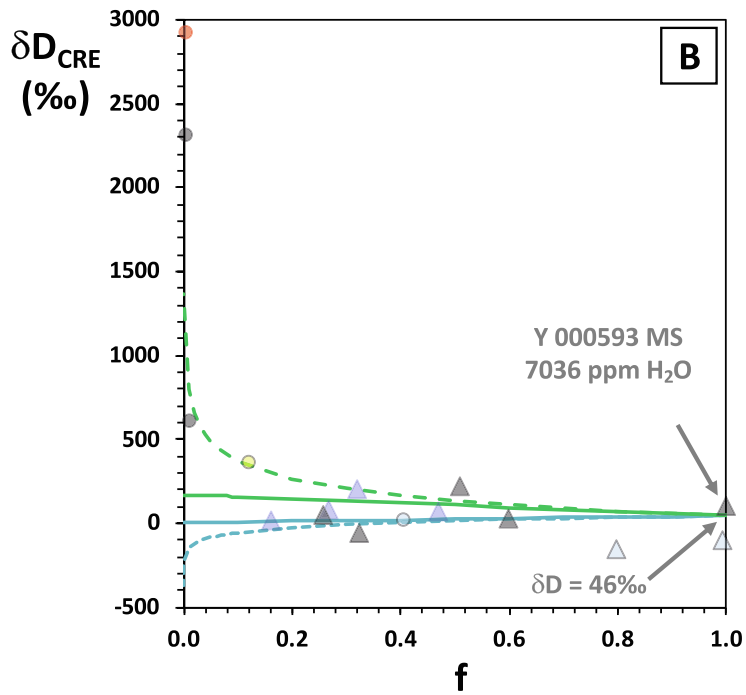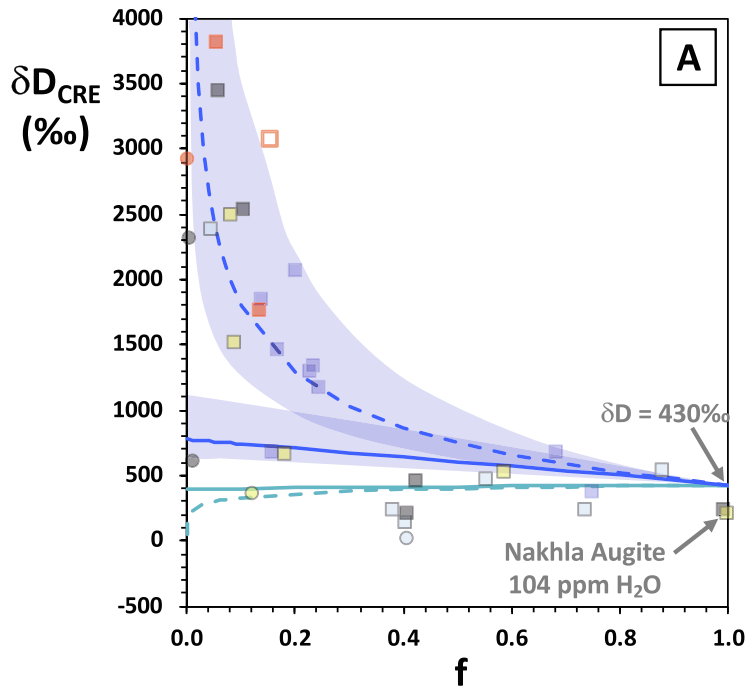

Fig. 10. One-dimensional modelling of hydrogen diffusion in clinopyroxene from a hydrothermal fluid or a melt at various temperatures. The hydrothermal fluid contains 50% H_2O and the nakhlite clinopyroxene grain initially contains 60 ppm H_2O (grey dotted curve). Minimal H is added to the clinopyroxene 1 μm outer edge if diffusion occurs at the average temperature at the Mars surface of −43 °C, even after 1.3 Ga, the crystallization age of nakhlites (blue dotted curve). If diffusion is allowed to last for 5 My at 50 °C (black curve) or if temperature is increased to 150 °C and diffusion lasts 500 years (orange curve), the water content of the pyroxene is affected within 200 μm of the edge. At the temperature of 700 °C, however, the water content of a 1 mm large clinopyroxene in contact with a melt containing 3640 ppm H_2O can gain 10 times its initial water content within a day (red curve). (For interpretation of the references to colour in this figure legend, the reader is referred to the web version of this article.)

the augites). These competing processes likely mitigated the potential diffusive intake of H by the pyroxenes.

A final test for interaction of the augites with hydrothermal fluids is to examine elements that are mobile in fluids: B, As, Sb, Tl, Pb, Mo, Sn are elements diagnostic of hydrothermal processes, and alkalis and U are markers of metasomatism by fluids (Noll et al., 1996; Scholten et al., 2018). Potassium, Rb, Na, Mo and Sb in pyroxene are too close to the detection limit of our LA-ICP-MS measurements to be used, but Na_2O measured by electron microprobe and B and Pb abundances by LA-ICP-MS were used to assess fluid mobility. The water content of augites, however, does not correlate with any of these fluid-mobile elements (B, Na_2O or Pb shown in Fig. SI7D-F). At the scale of individual pyroxene grains, fluid-mobile elements are enriched at the edge compared to the interior of the NWA 998 pigeonite (Fig. 5) and of the water-rich augite from NWA 6148 (Fig. 6). These elements being incompatible, their enhanced concentrations at the pyroxene edges could be the result of growth from an evolving melt being progressively enriched in incompatible elements as the crystallization proceeds, consistent with the model of crystallization from a fast-cooling evolving melt of Richter et al. (2016). In contrast, in a water-rich augite from Nakhla, the concentrations of the fluid-mobile elements B and Pb are low and show no variation (Fig. 3). In water-poor pyroxenes, however, the fluid-mobile elements B, Tl and Pb appear depleted at the water-poor edges (Fig. 7C–F). The lack of consistent correlations between water and fluid-mobile elements at the edges of individual pyroxene grains signifies that water was not added to the augites by the hydrothermal fluids that may have interacted with the intercumulus melts.

It should be noted that the edges of augite grains are enriched in Li compared to their interior in Nakhla and NWA 6148 augites (Figs. 3 and 6) although this is a little ambiguous in an augite from Y 000593 (Fig. 4). Lithium diffuses almost as fast as H in pyroxene (Coogan et al., 2005; Richter et al., 2014). Moreover, no correlation is observed between Li and water contents or with δD (Fig. 7G). These observations are consistent with previous results on nakhlites MIL 03346 and NWA 817, and are interpreted as diffusion of Li from the intercumulus melt into the edges of already crystallized pyroxenes during a final fast cooling stage (Richter et al., 2016). This Li exchange may have been contemporary to exposure to hydrothermal activity at the surface of Mars. Alternatively,

the source of the Li may also be igneous, given that the mesostasis is not enriched in Li relative to the pyroxenes and Li is incompatible during crystallization processes (Brenan et al., 1998; Fig. 7G).

The conclusion is that the nakhlite inter-cumulus melt likely interacted with hydrothermal fluids. However, the range of δD and water content of nakhlite pyroxene cores was likely not caused by interaction with martian surficial fluids with high δD or martian crustal fluids with low δD.

4.4. Magmatic processes

4.4.1. Degassing

4.4.1.1. Degassing of the nakhlite melts. When magmas reach upper crustal levels, the solubility of volatiles drops dramatically and they exsolve a gas phase (e.g., Sparks et al., 1994) during which water loss and fractionation of H isotopes can occur (De Hoog et al., 2009; Sharp, 2017a; Taylor and Sheppard, 1986). Both melt and their crystal cargoes degas contemporaneously. To model melt degassing (details in SI5), we chose as initial water content that of the most water-rich mesostasis (Y 000593A with 7036 ppm H_2O) and the average δD of the mesostasis measured in nakhlites (46‰). These values appear a reasonable estimate of the least degassed melt because they are similar to those of a melt in equilibrium with the most water- and Mg-rich augites (6883 ± 28 ppm H_2O and a δD of 430 ± 172‰; see Section 4.5). Using Eq. (SI8) that calculates the fractionation factor for a melt degassing water as H_2O and OH (De Hoog et al., 2009), generates an $\alpha_{vapor-melt} = 1.04$. Degassing models of a melt result in a decrease in δD of up to 40–422‰ (closed and open system respectively, light blue curves Fig. 11B). Although the curves match reasonably the range of δD of the mesostasis (382‰ difference between highest and lowest δD), some mesostasis analyses have too high or too low δD for their water content relative to these degassing models. This may be due, as discussed above, by the ingress of hydrothermal fluids into the intercumulus melt.

Evidence for a pyroxene crystallizing from a degassing melt, however, is seen at the scale of a single augite grain from NWA 6148 (Fig. 6). Both water contents and δD decrease toward the more Fe-rich edge of the pyroxene, while Li content increases. This could be explained by the pyroxene crystallizing from a fast degassing melt, or by the edges of the pyroxenes exchanging Li and H with a melt being rapidly depleted in water via degassing. However,

---

◄

Fig. 11. Degassing models and effect on δD. The variation of δD during degassing is calculated using Eq. (SI4) (closed system) and SI5 (open system). f is the proportion of water left in the degassing phase. The starting water contents to which f is normalized to are those of a water-rich least degassed Mg-rich augite in Nakhla (A) and of the most water-rich mesostasis (from Y 000593) (B). α is the fractionation factor and incl. = inclusion. The degassing modelling labelled "H_2O-OH in melt" (light blue curves) illustrates degassing via hydroxyl and water molecules diffusive loss from the melt (De Hoog et al., 2009) and a fractionation factor f calculated from Eq. (SI8). The degassing curves labelled H-D in px (bright blue curves) were calculated using a fractionation factor of 0.87 from Eq. (SI7) assuming faster diffusion for H relative to D in pyroxene. Fractionation of H isotopes during fluid-melt interaction at 700 °C to simulate a high-temperature hydrothermal system (green curves) is also shown with fractionation factors from Eq. (SI6) and Dalou et al. (2015) parameters. The low water content and high δD in most nakhlite pyroxenes and some of their melt inclusions are best explained by H loss via degassing through already crystallized pyroxene. The range of δD of the mesostasis likely resulted from both melt degassing and hydrothermal interaction. (For interpretation of the references to colour in this figure legend, the reader is referred to the web version of this article.)

degassing alone is not sufficient to explain the range of δD values exhibited by this augite. To calculate the extent of melt degassing that would have caused a drop from 92 to 58 ppm H_2O in the augite, we calculated the water content of melts in equilibrium with these augites (10,000–6000 ppm H_2O) using the pyroxene-melt partition coefficient of O'Leary et al (2010). Using the melt degassing model illustrated in Fig. 11B (light blue lines), this 40% decrease in the water content of the melt corresponds to a δD decrease of up to 20‰. This number is lower than the decrease in δD (~300‰) observed in the NWA 6148 augite. An additional mechanism must have lowered the δD of the melt to 247‰, again possibly the ingress into the melt of martian crustal fluids with low δD (Agee et al., 2013).

The Fe-rich edge of the augites likely formed (by crystallization or melt-rock reaction) at the same time as the mesostasis which represents the last part of the melt to crystallize. Whether the mesostasis is in equilibrium for water with the Fe-rich pyroxenes can be tested. A temperature of 1000 °C is used to calculate a $K_D^{Fe/Mg}$ of 0.48 (Grove and Bence, 1977) and obtain the MgO/FeO ratio of melts in equilibrium with the Fe-rich pyroxenes (i.e. late stage crystallization). The water content of melts in equilibrium with the more evolved pyroxenes are higher than those measured in the mesostasis (Fig. 9A). This discrepancy could have arisen from the mesostasis crystallizing from more degassed melts, or from more rapidly degassing melts, than the pyroxenes did. However, the analyses of the mesostasis were performed on NWA 6148, MIL 03346 and Y 000593, while the evolved pyroxenes were measured in Nakhla and NWA 998, and so the two data populations may not be directly comparable. Nevertheless, the water content of the mesostasis of Y 000593 shown in Fig. 4 (taken as that of the feldspar which is the major phase) correlates positively with its MgO/FeO ratio (Fig. 9A; $R^2 = 0.83$). During crystallization of a melt, the water content should increase due to the incompatibility of water and Mg# should decrease in crystallizing phases. The fact that the opposite is observed here is consistent with the intercumulus melt extensively degassing as crystallization proceeds, i.e. losing water faster than can be accumulated from crystallization processes. Moreover, the mesostasis analyses reveal decreases in δD of 100‰ towards the edge of the mesostasis (Fig. 4). This could be explained by solidification from a melt undergoing open-system degassing near grain boundaries (light blue curve in Fig. 11B). Evidence for degassing of the intercumulus melt of nakhlites is consistent with the degassing scenario invoked to explain their apatite volatile compositions (McCubbin et al., 2013).

A similar correlation between water content and major element may be seen in the mesostasis of MIL 03346 (Fig. 9A). However, in this case, the major element composition reflects that of the phases analyzed. In MIL 03346, lower Mg# and water content characterize the part of the mesostasis dominated by Fe-Ti oxides relative to that dominated by Na-rich glass, Fig. SI5. In NWA 6148, the MgO/FeO ratio is that of an average of all electron microprobe analyses of that mesostasis area (i.e. a mix of mainly feldspathic glass and Fe-Ti oxides, Fig. SI4A).

Finally, melt degassing could be in part responsible for the relatively low δD of the mesostasis (average 47 ± 117‰) relative to that of the Mg- and water-rich pyroxenes (average 430 ± 172‰; Fig. 2B; see Section 4.4.2). The pyroxenes crystallized first acquiring the δD of the melt they crystallized from. The mesostasis crystallized later, from the intercumulus liquid that had degassed and therefore had a lower δD (Fig. 11B).

4.4.1.2. Degassing of nakhlite pyroxenes. Pyroxenes also degas during the ascent of a crystal-loaded melt because of the lower solubility of H in pyroxene with decreasing pressure and the preferential partitioning of H into a gas or melt relative to a nominally anhydrous mineral (e.g., Bromiley et al., 2004; Aubaud et al., 2004; Grant et al., 2006). However, a decrease in δD with decreasing water content as generated by modeling the degassing of a melt (light blue lines in Figs. 11A and 2B) is the opposite of what is seen in the nakhlite pyroxene trend to water contents <30 ppm H_2O (Fig. 2). Instead, another mechanism of diffusion must be at play for pyroxenes. In pyroxenes, water is incorporated as protons (H) in lattice defects (primarily vacancies) and bound to structural oxygen (Skogby et al., 1990). Diffusion through pyroxene occurs as H and its rate is limited by the diffusion rate of vacancies. A mm-sized pyroxene can lose most of its H in a few hours at magmatic (≥800 °C) temperatures (Ingrin and Blanchard, 2006; Ferriss et al., 2016). Diffusion experiments show that the kinetics of H-D exchange can be 5 to >100 times faster than that of H loss or gain in diopside at low Fe contents, but that at higher Fe contents, they are the same (Hercule and Ingrin, 1999; Ingrin and Blanchard, 2006). These experiments, however, were done on diopsides containing significantly less Fe (Mg# ≥ 96.4) than nakhlite clinopyroxenes (Mg# = 50–62). We could speculate that at the higher Fe content of nakhlite pyroxenes, the diffusion of H is faster than D. It may thus be relevant to use a fractionation factor approximated by using the respective atomic masses of H and D (Eq. (SI7) using w_D and w_H; $\alpha_{vapor-cpx} = \sqrt{w_H/w_D} = 0.71$). Moreover, degassing experiments in garnet that, like pyroxene, is a nominally anhydrous mineral, show extreme kinetic fractionation of the H isotopes that can only be modeled by such a fractionation factor (Roskosz et al., 2018). A similar fractionation of H isotopes is observed during H loss from (nominally anhydrous) silica (Roskosz et al., 2016). To model pyroxene degassing (details in SI5), we chose as initial water content that of the most water- and Mg-rich augite (Nakhla Px6B with 104 ppm H_2O) and the average δD of the most Mg-rich augites with δD < 700‰ (430‰, see Section 4.4.2). Using $\alpha_{vapor-cpx} = 0.71$, the δD of most of the pyroxenes with low water content can be matched by a range of closed (with Eq. (SI4)) and open system (with Eq. (SI5)) degassing models with loss of >80% of their H (bright blue curves in Figs. 2B and 12A). As with the experimentally dehydrated garnet of Roskosz et al. (2016), the fractionation factor for pyroxene is likely not exactly of pure kinetic origin, i.e. depending solely on the atomic masses of H and D, but will vary with mineral composition. Bracketing the H

data of the nakhlite augites, we obtain a fractionation factor of 0.5–0.8 (SI5, shaded blue area in Fig. 11A).

This process of degassing from already crystallized pyroxene can be observed at the scale of individual pyroxene grains in the nakhlites. A lack of correlation with major elements is most consistent with degassing because H is one of the fastest diffusing elements through pyroxene while major elements are orders of magnitude slower (Ingrin and Blanchard, 2006; Cherniak and Dimanov, 2010). In particular, the incorporation of H in pyroxene is favored by the presence of Al (e.g., Aubaud et al., 2004; Hauri et al., 2006; Tenner et al., 2009). If no degassing occurred, crystallization from an evolving melt should result in enhanced contents of Al and H at the edge of a pyroxene because they are both incompatible elements and because the partition coefficient of H between melt and solid increases with the pyroxene Al content. Most of the nakhlite pyroxenes analyzed here, however, show the opposite: despite the increase in Al content at the edge of the augites, most evidence a decrease in water content. For example, FTIR measurements of augites from NWA 6148, MIL 03346 and NWA 998 (Fig. 7) show lower water contents in the edges of grains compared to their interiors, uncorrelated with major and trace element contents, and consistent with H loss during degassing. Similarly, in a pyroxene from Y 000593 (Fig. 4), the Mg# decreases and the Al content increases at the edge of the pyroxene, consistent with crystallization processes. However, the water content decreases at the edge and the analysis closest to the edge records a δD of 2459‰. This is consistent with degassing after the pyroxene, including its Fe-rich edge, was already crystallized.

Another example is the pyroxene from NWA 998 shown in Fig. 5. This pigeonite likely formed later than the ubiquitous augite in the nakhlite crystallization sequence, maybe due to a pressure decrease during crystallization (Treiman and Irving, 2008). The decrease in water content (from 380 to below detection limit for the SIMS) and increase in δD (to 3032‰ for the lowest detectable water content of 16 ppm H_2O) while the Mg# stays relatively constant is consistent with degassing of that pigeonite. The Al_2O_3 content also decreases towards that edge but not significantly enough to explain the decrease in water content. Given that the spatial context of the pigeonite grain we analyzed is lost, it is difficult to interpret its compositional variations. But the high-water content end of the profile may have been at the core of the pigeonite (likely broken in sample preparation) while the low-water content edge may represent a true edge that may have been adjacent to mesostasis.

4.4.1.3. Degassing of the inclusions. The water content of the melt inclusions found in pyroxene is higher than that of the pyroxene they are found in, consistent with water being incompatible in a melt relative to pyroxene. The two inclusions (Fe-rich pyroxene + Fe-Ti oxide) in an augite from Y 000593 have low water contents and high δD (40 ppm H_2O, 2327‰ and 83 ppm H_2O, 619‰; Fig. 2, SI3A). The enclosing augite from Y 000593 contains ≤1 ppm H_2O. These H compositions can be explained by degassing of the crystallized melt inclusions through their host pyroxene (bright blue lines in Fig. 11B). The other melt inclusions, from

augites in Nakhla and NWA 6148, have higher water contents and lower δD (862 ppm H_2O, 364‰ and 2862 ppm H_2O, 22‰, respectively; Fig. 2, SI4B and SI6). The melt inclusion from NWA 6148 has water content, δD (Fig. 2), texture and mineralogy (Fig. SI4B) similar to that of the mesostasis, and may actually be mesostasis showing through an augite in the plane of the polished surface of the sample. Alternatively, if it is indeed a melt inclusion, it must have degassed while still molten because its δD is low (22‰; light blue degassing curves in Fig. 11B). The plagioclase inclusion in the water-poor part of the pigeonite from NWA 998 (Fig. 5) also has low water content (26 ppm H_2O) and high δD (2894‰) consistent with open system degassing from the inclusion through the pyroxene (bright blue lines in Fig. 11B). A final observation is the water content being below detection limit in a pyroxene inclusion in a Nakhla olivine, consistent with H loss via degassing of that inclusion through the olivine.

Another test of degassing for the melt inclusions is to calculate whether they are in equilibrium for water with the Mg-rich augites. Melt inclusions may indeed represent trapped melt similar to that from which the first augites crystallized. The water content of melts in equilibrium with the undegassed pyroxenes (high water contents, low δD) is calculated, using the measured pyroxene compositions and the partition coefficients from Eq. (10) of O'Leary et al. (2010; Table SI5). The water contents of the melts are plotted versus their Mg/Fe ratio (Fig. 9B). The Mg/Fe ratio of the melt in equilibrium with pyroxenes is calculated using the $K_D^{Fe/Mg}$ between pyroxene and melt as a function of temperature (Grove and Bence, 1977). A temperature of 1250 °C is used for the Mg-rich augite ($K_D^{Fe/Mg}$ of 0.62) because augite was stable at that temperature in experiments reproducing Nakhla's composition (Longhi and Pan, 1989). The MgO/FeO ratio of the melt in equilibrium with the plagioclase inclusion found in a NWA 998 augite is calculated using the $K_D^{Fe/Mg}$ between plagioclase and melt of 1.4 (Longhi et al., 1976). The water content of melts in equilibrium with the earliest crystallized pyroxenes are higher than those measured in the melt inclusions in each nakhlite (Fig. 9B), consistent with degassing. Even the melt inclusion from a Nakhla augite that has relatively high water content and low δD (862 ppm H_2O and 364‰; Fig. SI6) has a slightly lower water content than melts in equilibrium with the Mg-rich undegassed Nakhla augites (Fig. 9B), i.e. recording degassing. This inclusion is also located in an augite with only a few ppm H_2O (Table SI1), i.e. that likely sustained degassing. The water content and δD of melt inclusions analyzed in this study all indicate degassing and therefore cannot be used to calculate those of the parent melts of the nakhlites.

4.4.1.4. Degassing of olivine?. The reason why the nakhlite olivines contain undetectable water is probably the result of the same crystallization and degassing effects as exemplified by the pyroxenes. As detailed in SI7, loss of H from olivine by degassing is compounded by the low solubility of H in olivine at low pressure, and the low compatibility of H in olivine compared to pyroxene (Demouchy et al., 2006; Peslier et al., 2008, 2015; Peslier and Luhr, 2006; Férot

and Bolfan-Casanova, 2012; Hauri et al., 2006; Tenner et al., 2009; Withers et al., 2011). The 320 ppm H_2O detected in the olivines of Y 000593 is likely from the inclusions of clinopyroxene that are abundant in these olivines (SI7; Fig. SI3B).

4.4.2. Crystallization

The augites were the first phases to crystallize from the nakhlites and correlations of incompatible trace elements

and Al_2O_3 content or Mg# within each augite reflect crystallization processes (Fig. SI7A and B). Recent modelling showed that the generally homogeneous major-element composition of the interior of the augites resulted from crystallization in a slow (years) cooling episode, rather than re-equilibration with the melt because Fe-Mg diffusion in augite is too slow within that time span (Richter et al., 2016). The interpretation of the Fe-rich rims is debatable. Richter et al. (2016) argue that the Mg-Fe exchange in
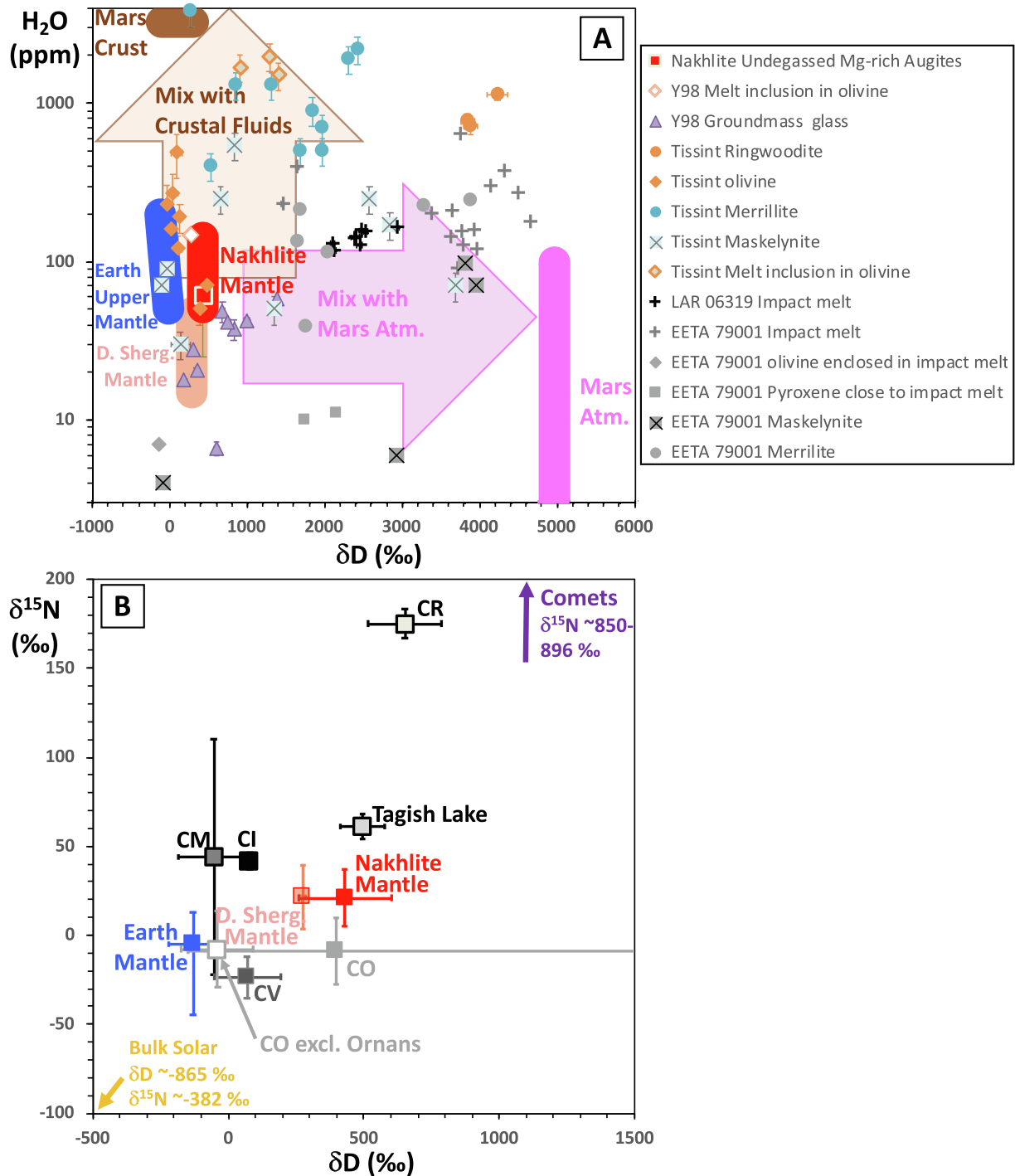
augite is too slow to have caused the Fe-rich rims of nakhlite augites, thus the latter are likely due to crystallization from an evolving melt during a fast cooling stage. On the other hand, the fact that REE concentrations do not systematically increase at the edges of augites (Ce shown in Figs. 3, 4 and 7E, F) is more compatible with an Fe-rich fluid interacting with the pyroxene edges. In any case, the Ti/Al ratio of the interior of the augites (Fig. SI7C) can be used to infer the pressure of crystallization (Nekvasil et al., 2004). This method can be applied here because the parental magma of chassignites, thought to be related to nakhlites (McCubbin et al., 2013), may be alkalic in composition (Nekvasil et al., 2007), i.e. similar in composition to the experiments used to calibrate the augite Ti/Al ratio with pressure (Nekvasil et al., 2004). Second, this method is valid only if no plagioclase crystallizes, which is ensured by selecting the augites with Mg# > 59, i.e. early enough in the crystallization sequence that it is unlikely that plagioclase had started forming. The resulting pressures at which the most magnesian augites crystallized are 0.93–0.43 GPa (Fig. SI7C). This correspond to depths in Mars of 78–36 km, i.e. at the base of the crust (Zuber et al., 2000). Note that this is not in contradiction with cumulate formation, crystallization of the Fe-rich rim of the augites and of the olivines, and cooling, at shallower depths (Harvey and McSween, 1992; Day et al., 2006; Lentz et al., 2011; McCubbin et al., 2013; Udry and Day, 2018). It only shows that the nakhlite augites started to crystallize at depths corresponding to the lower crust.

The fact that Nakhla and Y 000593 have more primitive augites (higher Mg#, lower Al and lower incompatible trace element contents, Fig. SI7) than the other nakhlites is likely a consequence of magma chamber processes. This is unrelated to their intermediate cooling rates relative to NWA 998 (slowest rates, rare mesostasis; Treiman and Irving, 2008) and MIL 03346 and NWA 6748 (fastest rates and most abundant mesostasis; Day et al., 2006; Jambon et al., 2016) which are due to eruption processes at the surface of Mars, possibly different lava flows of various thicknesses (Richter et al., 2016; Balta et al., 2017; Cohen et al., 2017; Udry and Day, 2018). Ascent of the nakhlite augite-laden magma resulted in degassing. Eruption at the surface was followed by rapid cooling (Richter et al., 2016), which as discussed previously, was not enough time for the core of the augites and the intercumulus melt to exchange water and Li, the fastest diffusing elements in that mineral.

Augites in Nakhla appear to have preserved evidence for crystallization processes, including in their water contents. Nakhla augites display a positive correlation between H_2O and Al_2O_3 content (Fig. 8B) and negative correlations with Mg# (Fig. 8A), CaO, and Cr_2O_3 contents. These correlations are controlled by analyses of one augite grain from Nakhla, where an increase in water, Fe and Al contents and a decrease in δD towards the Fe-rich edge of the pyroxene can be observed (Fig. 3). Apparently in this crystal, the melt, and the augite crystallizing from it, became progressively enriched in Fe and in Al, the latter promoting the incorporation of H. Alternatively, given that H and Li are both fast diffusers, and because the edge of the augite is enriched both in H and Li, diffusion of Li (Richter et al., 2016) and H from the melt into the edge of the Nakhla augite is possibly responsible. Despite the fact that H isotopes should not be fractionated during crystallization, the Nakhla augite exhibits a lowering of δD towards its Fe-rich edge (Fig. 3). Degassing of the melt while pyroxenes are crystallizing could explain the decrease in δD (as predicted; Fig. 11). But the rimward increase in water content could indicate this degassing must have been a slow event, allowing crystallization processes to result in increased water content in the differentiating melt and in the augite edges that crystallized from it (Fig. 8C).

Terrestrial pyroxenes, including undegassed phenocrysts, show a general range in H_2O contents of ~40–440 ppm (Peslier et al., 2002, 2012, 2017; Peslier, 2010; Xia et al., 2013; Liu et al., 2015; Peslier and Bizimis, 2015; Lloyd et al., 2016). The most H-rich nakhlite augites fall in this range of water contents. In addition, these water-rich augites have δD < 700‰, significantly lower than in the H-poor pyroxenes (Fig. 2). Thus, we interpret the water-rich augites as having undergone minimum degassing. There are some exceptions, in that two augites, in MIL 03346 (16 ppm H_2O) and in Nakhla (19 ppm H_2O), have

Fig. 12. (A) Average water content (ppm H_2O) versus δD (‰) of the undegassed most-Mg-rich augites from Nakhlites compared to those of various phases from shergottites Tissint, LAR 06319 and EETA 79001. Only samples not prepared in epoxy were selected from the literature (Usui et al., 2015; Mane et al., 2016; Hallis et al., 2017; Liu et al., 2018), the only exception being the melt inclusion from Y 980459 (Usui et al., 2012). Departure from martian mantle values is caused by a combination of mixing with atmosphere H during shock and of mixing with crustal fluids during shock and hydrothermal processes, in addition to degassing. Also shown are the estimated water content and δD of the nakhlite mantle (this study), depleted shergottite (D. Sherg) mantle (Usui et al., 2012), martian crust (Agee et al., 2013), martian atmosphere (Owen et al., 1988) and the shallow part of the Earth's upper mantle (Deloule et al., 1991; Michael, 1995; Sobolev and Chaussidon, 1996; Bell and Ihinger, 2000; Dixon et al., 2004; Shaw et al., 2012; Sarafian et al., 2015). The martian crust values are taken as those of the martian breccia meteorite NWA 7034 (Agee et al., 2013). (B) Hydrogen (δD in ‰) and nitrogen ($\delta^{15}N$ in ‰) isotopes of the martian mantle compared to those of the Earth's mantle (Deloule et al., 1991; Bell and Ihinger, 2000; Shaw et al., 2012; Cartigny and Marty, 2013; Hallis et al., 2015; Peslier et al., 2017) and of bulk carbonaceous chondrites (Kerridge, 1985; Alexander, 2017). The nitrogen isotope data on shergottites and nakhlites are from Mathew and Marti (2002, 2004, 2005) and Mathew et al. (2003). The shergottite mantle δD derives from that of a melt inclusion from depleted shergottite (D. sherg.) Y 980459 (Usui et al., 2012). The range of δD for the Earth's mantle may get as low as −218‰ (Hallis et al., 2015). Two estimates for CO chondrites are given, one with, and one without, meteorite Ornans which has exceptionally high δD (Kerridge, 1985). Bulk solar and comets δD and $\delta^{15}N$ are also shown (Geiss and Gloeckler, 1998; Hartogh et al., 2011; Marty et al., 2011; Altwegg et al., 2014; Bockelée-Morvan et al., 2015; Alexander, 2017). Comets have too high δD and $\delta^{15}N$ to be the source of water of Mars and Earth interiors. Carbonaceous chondrites-like planetesimals instead are the best candidates for the origin of Mars and Earth volatiles. The δD and $\delta^{15}N$ of the martian mantle resembles that of CO and Tagish Lake carbonaceous chondrites. The δD of the Earth mantle is significantly lower and closest to that of CM chondrites.

relatively low water contents despite having δD < 700‰. Overall, the water contents in the least-degassed, most water-rich, augites range from 16 to 270 ppm H_2O. The average water content of the most Mg-rich augites that have no evidence for degassing (red ellipse in Fig. 8) is 61 ± 36 ppm H_2O. Weis et al., 2017 rehydrated experimentally at 700 °C and 2 kb three Mg-rich augites from Nakhla that contained <10 ppm H_2O. The resulting water content of 130 ppm H_2O (orange square in Fig. 8A and B) is slightly higher than that measured in our undegassed Mg-rich Nakhla augites. The hydrothermal rehydration procedure may thus have added 30–50% more water than the original igneous water content of the augite prior to their degassing. Finally, one augite from Nakhla was measured by SIMS to have 97 ppm H_2O (Hallis et al., 2012a). Although no major element data is available from that study, this water content is similar to ours for Nakhla augites at Mg#~63.

Finally, four separate nakhlites contain "water-rich", Mg-rich, augites with δD < 700‰ (Fig. 9), independently of their position in nakhlite flows deduced from their cooling rates (Fig. SI7; e.g. Udry and Day, 2018). If the nakhlites had been generated from different parent melts, difference in water contents and δD would be expected in these pyroxenes, inherited from source heterogeneities. Instead our data is consistent with the hypothesis that all nakhlites have a common origin in space and time.

4.5. In search of the water content and δD of the martian mantle

4.5.1. Low δD, high Mg# augites: crustal or mantle H signature?

Whether the water content and δD of the least degassed Mg-rich augites (61 ± 36 ppm H_2O and 430 ± 172‰) can be used to infer those of the martian mantle is a matter of debate. One possibility is the model of McCubbin et al. (2013) and Shearer et al. (2018), based on analyses of Cl and F in apatites, for the magmatic history of the nakhlite-chassignite suite in three steps: (1) the olivines of the chassignites crystallize from a mantle melt, trapping some of it in their melt inclusions; (2) the melt in the magma chamber assimilates crustal Cl-rich hydrothermal fluids, (3) the nakhlite pyroxenes crystallize from this magma. If correct, the δD and water content of the nakhlite pyroxenes have a crustal origin. Apatites from the mesostasis record the interaction of the mesostasis melt with Cl-rich hydrothermal fluid and its degassing in both Chassigny and nakhlites (McCubbin et al., 2013; Shearer et al., 2018). Only apatites from Chassigny melt inclusions have mantle Cl-isotope signature, while no apatite from a nakhlite melt inclusion has been analyzed (Shearer et al., 2018). The validity of this model depends on the timing of addition of the Cl-rich hydrothermal fluids, before or after augite crystallization.

A contrasting model posits that nakhlite augites began to crystallize shortly after the chassignite olivines and prior to infiltration of Cl-rich hydrothermal fluids. In that case, the interior of the augites would record mantle δD and water contents. The pressures of crystallization calculated from the Ti/Al ratio of augite interiors (Fig. SI7C) suggest crystallization

at the bottom of the crust, likely too deep for interaction with surface hydrothermal fluids. The interpretation of Pb isotope data on the various nakhlite phases also seem consistent with this scenario. Lead "ages" recorded by a Nakhla apatite (3.95 Ga, Udry and Day, 2018) as well as by an isochron from Chassigny mineral fractions (4.4 Ga; Bellucci et al., 2016) are significantly older than the crystallization age of the nakhlites (1.3 Ga), indicating resetting of Pb isotopes since crystallization. More importantly, a Pb isochron from nakhlite main mineral fractions, including pyroxene fractions, records the same age as the crystallization age obtained using other isotopic systems (Bouvier et al., 2009). Consequently, in nakhlites, Pb isotopes do not appear disturbed in pyroxenes, while the apatite from the mesostasis records old ages inherited from surficial hydrothermal fluids. This favors the scenario of introduction of hydrothermal fluids in the nakhlites after crystallization of the pyroxene, and at the surface of Mars (Udry and Day, 2018). Until mantle signatures for Cl-isotopes can be found in nakhlite melt inclusions, the model of McCubbin et al. (2013) and Shearer et al. (2018) is speculative, primarily relying on analysis of the mesostasis. We proceed below with the assumption that the undegassed Mg-rich augites record mantle signatures.

4.5.2. A nakhlite source as hydrous as the shallow terrestrial mantle

The composition of the interior of the least-degassed, most Mg-rich augites can be used to calculate the water content of the nakhlite parent melt and, from it, that of the nakhlite mantle source (Table SI5). As detailed in SI8, the water content of the mantle source of nakhlites is calculated at 59–184 ppm H_2O. The range of water content for the source of chassignites (130–250 ppm H_2O), obtained from that of an amphibole in a melt inclusion in Chassigny (McCubbin et al., 2010), is mostly higher than that of the nakhlites. Perhaps this could indicate that some degassing took place between the crystallization of the chassignite olivines and that of the nakhlite augites, and therefore is not inconsistent with a common origin for chassignites and nakhlites. In contrast, the water contents of the depleted shergottite source (15–47 ppm H_2O), calculated from that of the Y 980459 melt inclusion with low δD (Usui et al., 2012), and of the enriched shergottite source (36–73 ppm H_2O), calculated from apatites (McCubbin et al., 2016), are lower than that of the nakhlites (Fig. 12A). These observations point to heterogeneities in the distribution of water contents in the mantle of Mars.

The water concentrations for the nakhlite source are overlapping, but display higher values than the range for the terrestrial mantle lithosphere (Fig. 12A; 50–100 ppm H_2O; e.g., Peslier et al., 2017), and lower values than that of Earth's upper asthenosphere (i.e. the source of mid ocean ridge basalts (MORB); 150–200 ppm H_2O; e.g., Michael, 1995; Sobolev and Chaussidon, 1996; Dixon et al., 2004; Sarafian et al., 2015). Given that Mars does not have a convective mantle, at present nor at the time of nakhlite formation 1.3 Ga ago, the most relevant comparison may be that with the terrestrial mantle lithosphere, i.e. a depleted upper mantle where heat is transferred conductively. Parts of the martian mantle may be slightly wetter (nakhlite source) or

slightly drier (depleted shergottite source) than the Earth's mantle lithosphere. The martian mantle composition is likely inherited from magma ocean processes (Brandon et al., 2000, 2012; Borg et al., 2003; Debaille et al., 2007) and its upper part may have been variably depleted in incompatible elements such as H during the overturn of magma ocean cumulates and crustal formation (Elkins-Tanton et al., 2003; Debaille et al., 2009; Breuer et al., 2016; Day et al., 2018). In any case, our results on nakhlites can only provide an estimate of the water content of the upper part of the Martian mantle, which, given uncertainties, has similar to or lower water contents than the upper part of the Earth's mantle. Given the solubility increase of H in olivine with pressure (Kohlstedt et al., 1996; Hirschmann et al., 2005; Bali et al., 2008; Ardia et al., 2012; Yang et al., 2014), which is observed also for relatively Fe-rich martian olivine compositions (Withers et al., 2011), water contents might be >200 ppm H_2O at deeper levels of the martian mantle compared to the presently modeled nakhlite source.

4.5.3. Comparison of δD in nakhlite and shergottite phases

The lower δD of the mesostasis and some of our melt inclusions in nakhlites is explained here by degassing processes, while the 430 ± 172‰ recorded in the Mg-rich undegassed pyroxenes may represent martian mantle values (Fig. 2). However, if the chassignites and nakhlites are related, degassing from the melt could have occurred between the time of the olivine crystallization and the start of the augite crystallization. In that case, the δD of the nakhlite undegassed pyroxenes would not represent a mantle value. Unfortunately, the only H isotopic microanalyses of chassignites were obtained on samples impregnated with epoxy. All hydrous phases (amphiboles, a biotite, an apatite) in melt inclusions from chassignites, which are more shocked than nakhlites (Floran et al., 1978; Fritz et al., 2005a; Bogard and Garrison, 2008; Fritz and Greshake, 2009; Treiman et al., 2007), record high δD (811–1880‰). This has been interpreted as resulting from exchange with fluids that interacted with the high-δD martian atmosphere (Watson et al., 1994; Boctor et al., 2003; Giesting et al., 2015). In contrast, glass in recrystallized melt inclusions from Chassigny olivines have lower δD (95–225‰, average 168 ± 54‰), with the exception of one glassy inclusion that may have been shock melted and records a δD of 1754‰ (Boctor et al., 2003). The lower δD were interpreted as possibly representing magmatic values, with hydrous phases having been more affected by crustal fluids than glass in melt inclusions (Boctor et al., 2003). If the above value of 168 ± 54‰ is representative of that of the chassignite parent melt, then it is lower than that of the nakhlites (430 ± 172‰). However, 168‰ is probably low compared to the true glass δD if there was contribution from epoxy during the SIMS analyses. Given this uncertainty, it is difficult to use these data to prove whether degassing occurred between the times olivine and pyroxene crystallized from the nakhlite-chassignite parent melt.

Martian meteorites other than nakhlites have all been significantly shocked. Their impact-affected phases systematically record high δD (see impact melts, ringwoodite,

most maskelynites in Fig. 12A), even in samples prepared in epoxy, and have been explained by shock implantation of martian atmosphere or incorporation of surface alteration (Boctor et al., 2003; Usui et al., 2012, 2015; Chen et al., 2015; Giesting et al., 2015; Mane et al., 2016; Hallis et al., 2017; Liu et al., 2018). In olivines from the heavily shocked (~35 GPa) olivine-phyric shergottite Tissint, and if only SIMS analyses performed on non-epoxied aliquots are selected (70–485 ppm H_2O, Fig. 12A), δD vary from 12 to 470‰ (Mane et al., 2016; Hallis et al., 2017). However, water solubility in olivine decreases significantly as pressure decreases (e.g., Kohlstedt et al., 1996; Hirschmann et al., 2005; Bali et al., 2008; Ardia et al., 2012; Yang et al., 2014), and therefore the water contents of olivine formed at low pressure (such as in Tissint) seem high for an igneous olivine. They were interpreted as "deuteric alteration during late stage crystallization" or as having interacted with crustal fluids (Mane et al., 2016; Hallis et al., 2017). Except for one melt inclusion from Y 980459 that has low δD (275‰), all melt inclusions measured in other shergottites, enriched and depleted, have high δD (>900‰; Fig. 12A; Usui et al., 2012; Hu et al., 2014; Mane et al., 2016). These have been interpreted as contaminated by crustal fluids that interacted with the martian atmosphere or as resulting from degassing (Usui et al., 2012; Mane et al., 2016). In any case, they do not represent martian mantle compositions. Studies of Tissint, a heavily shocked olivine-phyric shergottite which was observed falling, argue that either the low δD and water content of its maskelynites (−116 to 135‰, 30–70 ppm H_2O; Mane et al., 2016) or the low δD end-member of its impact melts (~0‰, Chen et al., 2015) reflect that of the shergottite mantle source. However, the potential effect of shock and degassing on these values is a concern as evidenced in the maskelynite of shergottite LAR 06319 (Dudley et al., 2019). Degassing has likely affected shergottites and specifically Tissint (McSween et al., 2001, Chen et al., 2015; Castle and Herd, 2017). Consequently, after reviewing the literature of hydrogen isotope measurements of martian meteorite phases, it appears that the most appropriate measurements for estimating the δD of the martian mantle remains the melt inclusion of depleted shergottite Y 980459 (Usui et al., 2012) and of the undegassed Mg-rich augites in the nakhlites analyzed here.

4.5.4. A higher δD for the martian mantle relative to that of Earth

Our estimation of 430 ± 172‰ ‰ for the source of nakhlites is higher than the δD of the Earth's mantle (−20 to −130‰; Fig. 12A; Deloule et al., 1991; Bell and Ihinger, 2000; Shaw et al., 2012; Hallis et al., 2015; Peslier et al., 2017). The key here is whether this difference is significant or if the δD values of the martian mantle extend to lower values and overlap those of the Earth's mantle. Two hypotheses to explain this difference are now explored: magma ocean and planetary formation processes.

4.5.4.1. Magma ocean processes.
The small size of Mars relative to Earth may have enhanced volatile loss during magma ocean crystallization (Elkins-Tanton, 2008;

Greenwood et al., 2008) and the resulting D/H fractionation produced a more elevated δD for the martian mantle relative to that of Earth, assuming their δD was similar after accretion. Large fractionation of H isotopes would be expected if water in the magma ocean degasses as H_2 (from Eq. (SI7) with the atomic weights of H_2 and DH, $\alpha_{atm\text{-}MagmaOcean} = 0.82$; Sharp et al., 2013). Degassing H_2O or OH results in less fractionation (at most a δD increase of 218‰ in an open system with $\alpha_{atm\text{-}MagmaOcean} = 0.97$ from Eq. (SI7) with the atomic weights of H_2O and DHO, or of OH and OD), and could not account for the $\sim$560‰ δD difference between Earth and Mars mantles. For the magma ocean to degas H_2 necessitates reduced conditions (Sharp et al., 2013). This is a reasonable assumption if the low oxygen fugacities (fO_2) recorded by the first crystallized phases of primitive shergottites ($\Delta FMQ \sim -4$ to -2, with oxygen fugacity expressed relative to the fayalite-magnetite-quartz buffer) are any indication of that of the magma ocean (Herd, 2003; Usui et al., 2008; Peslier et al., 2010; Balta et al., 2014; Castle and Herd, 2017). Interestingly, however, nakhlites are characterized by higher fO_2 ($\Delta FMQ \sim 0$) than shergottites (Dyar et al., 2005; McCanta et al., 2009; Szymanski et al., 2010). Pyroxene in Chassigny also has lower amounts of Fe^{3+}, which suggests lower oxygen fugacity during its crystallization, compared to nakhlites, although no exact number could be calculated (Dyar, 2003). The sources of nakhlites and shergottites could have different fO_2 inherited from magma ocean processes (McCanta et al., 2009). But now that the shergottite source appears drier than that of nakhlites, following a redox reaction ($Fe^{3+} + O^{2-} + \frac{1}{2}H_2 = Fe^{2+} + OH^-$) would predict the opposite, i.e. a more oxidized source for shergottites, if H is the main control of fO_2 in the martian mantle.

Two other processes can be explored to try and explain why nakhlites are more oxidized than shergottites: crystallization and degassing of their magma. Oxidation during crystallization has been evidenced in shergottites (Peslier et al., 2010; Castle and Herd, 2017), and could be in part responsible for the $\sim$1 log unit difference between the first crystallized phases (olivine, augite and melt inclusions) and the mesostasis (Fe-Ti oxides) of the nakhlite-chassignite suite. Nevertheless, it appears that the first crystallized phases of the nakhlites record higher fO_2 than those of the shergottites, even after taking crystallization into account (Dyar, 2003; Dyar et al., 2005). Another method of determining fO_2 in basalts is to use the Eu/Gd ratio of augites (Wadhwa, 2001). Using this method, it has been suggested that augites in NWA 998 record ΔFMQ -2 (Treiman and Irving, 2008). However, this method should not be applied to nakhlites because it requires to also know the Eu/Gd of their parent melt. The latter cannot be approximated by that of the whole-rock for three reasons: (i) nakhlites are cumulates (Harvey and McSween, 1992) and therefore their whole-rock Eu/Gd ratio is influenced by augite accumulation; (ii) their intercumulus melt has mixed with hydrothermal fluids (McCubbin et al., 2013) which Eu and Gd contents are not known; (iii) stones of paired nakhlites can have different amount of mesostasis (Udry et al., 2012), creating a range of whole-rock Eu/Gd ratios for each nakhlite. The second process that could

account for the oxidation of the nakhlites is that the strong degassing that we evidenced is also responsible for oxidizing their phases, following the Fe-H redox reaction, and that shergottites degassed less. It is not possible to know if that is the case at this point, although the low δD recorded in shergottite Tissint olivine (12–470‰; Fig. 12A; Mane et al., 2016) could mean that this first crystallized mineral did not experience H loss by degassing like most nakhlite pyroxenes. Degassed and undegassed pyroxenes should be analyzed for their Fe^{3+} contents in nakhlites to explore this hypothesis. More extensive degassing of the nakhlite melts relative to those of shergottites remains an unverifiable hypothesis. Given that we cannot prove whether the mantle source of nakhlites is as reduced as that of shergottites, a necessary requirement for H_2 degassing that would provide enough D/H fractionation, the hypothesis of more extensive degassing of the martian magma ocean relative to that of Earth to explain the higher δD of the martian mantle cannot be validated unambiguously.

Finally, to relax the conditions for a reduced magma ocean, another possibility is that the magma ocean, in addition to degassing and creating the martian atmosphere, exchanged H and D with it (Sharp, 2017b). The martian atmosphere may have had time to evolve to relatively high δD via H loss to space before complete solidification of the top of the magma ocean (Elkins-Tanton, 2008; Villanueva et al., 2015; Hier-Majumder and Hirschmann, 2017).

4.5.4.2. Planet formation. Mars and Earth accreted in different parts of the inner proto-planetary disk, and the difference in δD of their mantle could have arisen from slightly different types and/or relative proportions of material accreted in each. The δD of 430 ± 172‰ for the Martian mantle is consistent with results from dynamical modeling of accretion in the proto-planetary disk that predict δD of 200–600‰ for Mars (Lunine et al., 2003). An increasing gradient in δD with distance from the Sun is also suggested to exist and to be the result of a broad mix of solar nebula low δD (-865‰, Bulk Solar in Fig. 12B; Geiss and Gloeckler, 1998; Marty et al., 2011) and interstellar high δD (851‰), the latter being a significant component of cometary volatiles (Comets in Fig. 12B; Hartogh et al., 2011; Altwegg et al., 2014; Bockelée-Morvan et al., 2015; Piani et al., 2015; Alexander, 2017). Even if this simple model is controversial and has been applied so far to the origin of primitive materials (chondrites and comets; Yang et al., 2013; Horner et al., 2007), it would be consistent with our results given that Mars is further from the Sun than Earth (Sharp, 2017b). Earth would have more solar nebular component and Mars more outer solar component. It has indeed been argued that Earth could have preserved mantle reservoirs with H inherited from nebular accretion processes resulting in $\delta D < 218$‰ (Hallis et al., 2015). However, the low δD measured in pyroxene from eucrites (-241 ± 64‰; Stephant et al., 2016) seems to contradict this scenario given that these meteorites come from the asteroid belt, i.e. even further from the Sun than Mars.

Instead, Mars and Earth may have acquired their water after accretion while they were already differentiating (reviewed in Peslier et al., 2017). A planetary "grand tack"

scenario during disturbances of Jupiter's orbit at that time (Walsh et al., 2011; O'Brien et al., 2014) or the gas-giant planet formation (Raymond and Izidoro, 2017) could have propelled water-rich bodies like comets and carbonaceous chondrites into the inner "dry" Solar System. Comets have generally higher δD and nitrogen isotopic ratios ($\delta^{15}N$) than the Earth and martian mantle (Fig. 12B; Mathew and Marti, 2002, Mathew et al., 2003, Mathew and Marti, 2005; Marti and Mathew, 2004; Hartogh et al., 2011; Altwegg et al., 2014; Bockelée-Morvan et al., 2015), and in this scenario, could not be a source for water in the interior of Earth and Mars. Carbonaceous chondrite-like material has been suggested to have provided the water locked in the Earth's and Mars interiors because the ranges in δD and $\delta^{15}N$ of these meteorites overlap (Fig. 12B) and they contain significant amounts of water (Alexander et al., 2012; Alexander, 2017; Stephant et al., 2017). Here, as we evidence differences in δD between Mars and Earth's mantles, Mars may have acquired its water from CO- and Tagish Lake-like material while Earth acquired its water from a higher proportion of CM-like material (Fig. 12B).

5. CONCLUSIONS

Detailed in-situ analyses were performed on the igneous phases of a well-characterized group of clinopyroxenites from Mars, the nakhlites, that most likely originated from the same parent melt. The effect of shock was also largely ignored because nakhlites are minimally shocked. The nakhlite minerals analyzed here were prepared without epoxy or any other glue and polished without any lubricant. This allows confidence that the variations in water contents and δD reported are linked to processes that affected the meteorite and not to laboratory contamination. Combining major and trace element contents with water contents and δD together with spatial relationships at the scale of individual mineral grains allows to sort out the different processes that influenced the distribution of H and D in nakhlites.

The dominant process controlling H content and isotope distribution in nakhlites appears to be degassing. Fractionation of H isotopes during degassing of a H_2O-OH bearing melt results in a decrease in δD ($\sim300‰$ after most of the H has left the melt in an open system; light blue curves in Fig. 2B). This process likely contributed to the range of δD values and water contents of the mesostasis, although influx of crustal fluids with low δD into the intercumulus melt also influenced the mesostasis H composition. Melt degassing also in part explains the lower δD of the mesostasis (-60 to $230‰$) relative to that of the least degassed pyroxenes ($430 \pm 172‰$): the pyroxenes crystallized when the δD of the degassing melt was higher than when the phases of the mesostasis crystallized. Fractionation of H isotopes during degassing of pyroxene, on the other hand, results in a large δD increase ($\sim3000‰$ after most of the H has left the melt in an open system; bright blue curves in Fig. 2B). Most nakhlite pyroxenes have undergone degassing, explaining their low water contents and high δD (<20 ppm H_2O, $\delta D > 1000‰$). Inclusions in nakhlite pyroxenes also appear to have undergone degassing. The

lack of water in olivine resulted from a combination of degassing and low solubility and compatibility of H in that mineral.

The least degassed, most Mg-rich augites of the nakhlites analyzed here have a δD of $430 \pm 172‰$ which either represents an average crustal value or the δD of the nakhlite mantle source. The two possibilities depend on when the Cl-rich hydrothermal fluids interacted with the nakhlite melt, before or after pyroxene crystallization. The latter is our preferred scenario, in which case it can be calculated that the nakhlite mantle source has a δD of $430 \pm 172‰$ and a water content of ~60–185 ppm H_2O. The mantle source of the shergottites, the basaltic suite of martian meteorites, is estimated to have a similar δD within uncertainties ($275 \pm 10‰$; Usui et al., 2012) but a lower water content (15–46 ppm H_2O). The shallow part of the Earth mantle has similar water contents to the nakhlite and shergottite sources. The δD of the Earth's mantle (Bell and Ihinger, 2000; Deloule et al., 1991; Hallis et al., 2015; Peslier et al., 2017; Shaw et al., 2012), however, is significantly lower (-20 to $-130‰$) than that of Mars. The discrepancy between δD of Earth and Mars may have arisen from acquiring their water from different proportions of carbonaceous chondrite like planetesimals.

APPENDIX A. SUPPLEMENTARY MATERIAL

Supplementary data to this article can be found online at https://doi.org/10.1016/j.gca.2019.04.023.

REFERENCES

Agee C. B., Wilson N. V., McCubbin F. M., Ziegler K., Polyak V. J., Sharp Z. D., Asmerom Y., Nunn M. H., Shaheen R., Thiemens M. H., Steele A., Fogel M. L., Bowden R., Glamoclija M., Zhang Z. and Elardo S. M. (2013) Unique meteorite from early amazonian mars: water-rich basaltic Breccia Northwest Africa 7034. *Science* **339**, 780–785.

Albarède F. (2009) Volatile accretion history of the terrestrial planets and dynamic implications. *Nature* **461**, 1227–1233.

Alexander C. M. O. D. (2017) The origin of inner Solar System water. *Phil. Trans. R. Soc.* **A**, 375.

Alexander C. M. O. D., Bowden R., Fogel M. L., Howard K. T., Herd C. D. K. and Nittler L. R. (2012) The provenances of asteroids, and their contributions to the volatile inventories of the terrestrial planets. *Science* **337**, 721–723.

Altwegg K., Balsiger H., Bar-Nun A., Berthelier J. J., Bieler A., Bochsler P., Briois C., Calmonte U., Combi M., De Keyser J., Eberhardt P., Fiethe B., Fuselier S., Gasc S., Gombosi T. I., Hansen K. C., Hässig M., Jäckel A., Kopp E., Korth A., LeRoy L., Mall U., Marty B., Mousis O., Neefs E., Owen T., Rème H., Rubin M., Sémon T., Tzou C.-Y., Waite H. and Wurz P. (2014) 67P/Churyumov-Gerasimenko, a Jupiter family comet with a high D/H ratio. *Science*, 347.

Anders E. and Grevesse N. (1989) Abundances of the elements: meteoritic and solar. *Geochim. Cosmochim. Acta* **53**, 197–214.

Ardia P., Hirschmann M. M., Withers A. C. and Tenner T. J. (2012) H_2O storage capacity of olivine at 5–8 GPa and consequences for dehydration partial melting of the upper mantle. *Earth Planet. Sci. Lett.* **345–348**, 104–116.

Aubaud C., Hauri E. and Hirschmann M. M. (2004) Hydrogen partition coefficients between nominally anhydrous minerals and basaltic melts. *Geophys. Res. Lett.* **31**. https://doi.org/10.1029/2004GL021341.

Bali E., Bolfan-Casanova N. and Koga K. T. (2008) Pressure and temperature dependence of H solubility in forsterite: an implication to water activity in the Earth interior. *Earth Planet. Sci. Lett.* **268**, 354–363.

Balta J. B., Sanborn M. E., Udry A., Wadhwa M. and McSween, Jr., H. Y. (2014) Petrology and trace element geochemistry of Tissint, the newest shergottite fall. *Meteor. Planet. Sci.* **50**, 63–85.

Balta B. J., Sanborn M. E., Mayne R. G., Wadhwa M., McSween H. Y. and Crossley S. D. (2017) Northwest Africa 5790: a previously unsampled portion of the upper part of the nakhlite pile. *Meteor. Planet. Sci.* **52**, 36–39.

Barnhart C. J., Nimmo F. and Travis B. J. (2010) Martian post-impact hydrothermal systems incorporating freezing. *Icarus* **208**, 101–117.

Bell D. R. and Ihinger P. D. (2000) The isotopic composition of hydrogen in nominally anhydrous mantle minerals. *Geochim. Cosmochim. Acta* **64**, 2109–2118.

Bellucci J. J., Nemchin A. A., Whitehouse M. J., Snape J. F., Kielman R. B., Bland P. A. and Benedix G. K. (2016) A Pb isotopic resolution to the Martian meteorite age paradox. *Earth Planet. Sci. Lett.* **433**, 241–248.

Beran A. and Libowitzky E. (2006) Water in natural mantle minerals II: olivine, garnet and accessory minerals. In *Water in Nominally Anhydrous Minerals* (eds. H. Keppler and J. R. Smyth). Mineralogical Society of America, Chantilly, VA, pp. 169–191.

Berry A. J., Hermann J., O'Neill H. S. C. and Foran G. J. (2005) Fingerprinting the water site in mantle olivine. *Geology* **33**, 869–872.

Bibring J.-P., Langevin Y., Poulet F., Gendrin A., Gondet B., Berthé M., Soufflot A., Drossart P., Combes M., Bellucci G., Moroz V., Mangold N., Schmitt B. and team O. (2004) Perennial water ice identified in the south polar cap of Mars. *Nature* **428**, 627–630.

Bockelée-Morvan D., Calmonte U., Charnley S., Duprat J., Engrand C., Gicquel A., Hässig M., Jehin E., Kawakita H., Marty B., Milam S., Morse A. D., Rousselot P., Sheridan S. and Wirström E. (2015) Cometary isotopic measurements. *Space Sci. Rev.* **197**, 47–83.

Boctor N. Z., Alexander C. M. O. D., Wang J. and Hauri E. (2003) The sources of water in martian meteorites: clues from hydrogen isotopes. *Geochim. Cosmochim. Acta* **67**, 3971–3989.

Bogard D. D. and Garrison D. H. (2008) 39Ar–40Ar age and thermal history of martian dunite NWA 2737. *Earth Planet. Sci. Lett.* **273**, 386–392.

Borg L. E., Nyquist L. E., Wiesmann H., Shih C. Y. and Reese Y. (2003) The age of Dar al Gani 476 and the differentiation history of the martian meteorites inferred from their radiogenic isotopic systematics. *Geochim. Cosmochim. Acta* **67**, 3519–3536.

Bouvier A., Blichert-Toft J. and Albarède F. (2009) Martian meteorite chronology and the evolution of the interior of Mars. *Earth Planet. Sci. Lett.* **208**, 285–295.

Bradley J. P., Ishii H. A., Gillis-Davis J. J., Ciston J., Nielsen M. H., Bechtel H. A. and Martin M. C. (2014) Detection of solar wind-produced water in irradiated rims on silicate minerals. *Proc. Nat. Acad. Sci.* **111**, 1732–1735.

Brandon A. D., Walker R. J., Morgan J. W. and Goles G. G. (2000) Re-Os isotopic evidence for early differentiation of the martian mantle. *Geochim. Cosmochim. Acta* **64**, 4083–4095.

Brandon A. D., Puchtel I. S., Walker R. J., Day J. M. D., Irving A. J. and Taylor L. A. (2012) Evolution of the martian mantle inferred from the ^{187}Re-^{187}Os isotope and highly siderophile element abundance systematics of shergottite meteorites. *Geochim. Cosmochim. Acta* **76**, 206–235.

Brenan J. M., Neroda E., Lundstrom C. C., Shaw H. F., Ryerson F. J. and Phinney D. L. (1998) Behaviour of boron, beryllium, and lithium during melting and crystallization: constraints from mineral-melt partitioning experiments. *Geochim. Cosmochim. Acta* **62**, 2129–2141.

Breuer D., Plesa A.-C., Tosi N. and Grott M. (2016) Water in the Martian interior—the geodynamical perspective. *Meteor. Planet. Sci.* **51**, 1959–1992.

Bridges J. C. and Grady M. M. (2000) Evaporite mineral assemblages in the nakhlite (martian) meteorites. *Earth Planet. Sci. Lett.* **176**, 267–279.

Bridges J. C. and Schwenzer S. P. (2012) The nakhlite hydrothermal brine on Mars. *Earth Planet. Sci. Lett.* **359–360**, 117–123.

Bridges J. C., Catling D. C., Saxton J. M., Swindle T. D., Lyon I. C. and Grady M. M. (2001) Alteration assemblages in martian meteorites: implications for near-surface processes. *Space Sci. Rev.* **96**, 365–392.

Bromiley G. D., Keppler H., McCammon C. A., Bromiley F. A. and Jacobsen S. D. (2004) Hydrogen solubility and speciation in natural, gem-quality chromian diopside. *Am. Mineral.* **89**, 941–949.

Bunch T. E. and Reid A. M. (1975) The nakhlites, I Petrography and mineral chemistry. *Meteoritics* **10**, 303–315.

Burke D. J., Dukes C. A., Kim J.-H., Shi J., Famá M. and Baragiola R. A. (2011) Solar wind contribution to surficial lunar water: laboratory investigations. *Icarus* **211**, 1082–1088.

Carr M. H. and Head J. W. (2010) Geologic history of Mars. *Earth Planet. Sci. Lett.* **294**, 185–203.

Cartigny P. and Marty B. (2013) Nitrogen isotopes and mantle geodynamics: the emergence of life and the atmosphere–crust–mantle connection. *Elements* **9**, 359–366.

Cartwright J. A., Gilmour J. D. and Burgess R. (2013) Martian fluid and martian weathering signatures identified in Nakhla, NWA 998 and MIL 03346 by halogen and noble gas analysis. *Geochim. Cosmochim. Acta* **105**, 255–293.

Castle N. and Herd C. D. K. (2017) Experimental petrology of the Tissint meteorite: redox estimates, crystallization curves, and evaluation of petrogenetic models. *Meteor. Planet. Sci.* **52**, 125–146.

Chamberlin S., Christoffersen R. and Keller L. (2008) Space plasma ion processing of the lunar soil: modeling of radiation-damaged rim widths on lunar grains. In *Lunar and Planetary Science Conference XXXIX, Houston, TX*, p. 2302.

Changela H. G. and Bridges J. C. (2010) Alteration assemblages in the nakhlites: variation with depth on Mars. *Meteor. Planet. Sci.* **45**, 1847–1867.

Chassefière E. and Leblanc F. (2004) Mars atmospheric escape and evolution; interaction with the solar wind. *Planet. Space Sci.* **52**, 1039–1058.

Chen Y., Liu Y., Guan Y., Eiler J. M., Ma C., Rossman G. R. and Taylor L. A. (2015) Evidence in Tissint for recent subsurface water on Mars. *Earth Planet. Sci. Lett.* **425**, 55–63.

Cherniak D. J. and Dimanov A. (2010) Diffusion in pyroxene, mica and amphibole. In *Diffusion in minerals and melts* (eds. Y. Zhang and D. J. Cherniak). Mineralogical Society of America, Geochemical Society, Chantilly, VA, pp. 641–690.

Chiodini G., Marini L. and Russo M. (2001) Geochemical evidence for the existence of high-temperature hydrothermal brines at Vesuvio volcano, Italy. *Geochim. Cosmochim. Acta* **65**, 2129–2147.

Christen F., Eugster O. and Busemann H. (2005) Mars ejection times and neutron capture effects of the nakhlites Y000593 and Y000749, the olivine-phyric shergottite Y980459, and the lherzolite NWA1950. *Antarct. Meteorite Res.* **18**, 117–132.

Cockell C. S., Balme M., Bridges J. C., Davila A. and Schwenzer S. P. (2012) Uninhabited habitats on Mars. *Icarus* **217**, 184–193.

Cohen B. E., Mark D. F., Cassata W. S., Lee M. R., Tomkinson T. and Smith C. L. (2017) Taking the pulse of Mars via dating of a plume-fed volcano. *Nat. Commun.* **8**, 640.

Coogan L. A., Kasemann S. A. and Chakraborty S. (2005) Rates of hydrothermal cooling of new oceanic upper crust derived from lithium-geospeedometry. *Earth Planet. Sci. Lett.* **240**, 415–424.

Crozaz G., Floss C. and Wadhwa M. (2003) Chemical alteration and REE mobilization in meteorites from hot and cold deserts. *Geochim. Cosmochim. Acta* **67**, 4727–4741.

Dalou C., Le Losq C. and Mysen B. O. (2015) In situ study of the fractionation of hydrogen isotopes between aluminosilicate melts and coexisting aqueous fluids at high pressure and high temperature – implications for the δD in magmatic processes. *Earth Planet. Sci. Lett.* **426**, 158–166.

Day J. M. D., Taylor L. A., Floss C. and McSween, Jr., H. Y. (2006) Petrology and chemistry of MIL 03346 and its significance in understanding the petrogenesis of nakhlites on Mars. *Meteor. Planet. Sci.* **41**, 581–606.

Day J. M. D., Tait K. T., Udry A., Moynier F., Liu Y. and Neal C. R. (2018) Martian magmatism from plume metasomatized mantle. *Nat. Commun.* **9**, 4799.

De Hoog J. C. M., Taylor B. E. and Van Bergen M. J. (2009) Hydrogen-isotope systematics in degassing basaltic magma and application to Indonesian arc basalts. *Chem. Geol.* **266**, 256–266.

Debaille V., Brandon A. D., Yin Q. Z. and Jacobsen B. (2007) Coupled ^{142}Nd-^{143}Nd evidence for a protracted magma ocean in Mars. *Nature* **450**, 525–528.

Debaille V., Brandon A. D., O'Neill C., Yin Q.-Z. and Jacobsen B. (2009) Early martian mantle overturn inferred from isotopic composition of nakhlite meteorites. *Nat. Geo.* **2**, 548–552.

Deloule E., Albarède F. and Sheppard S. M. F. (1991) Hydrogen isotope heterogeneities in the mantle from ion probe analysis of amphibole from ultramafic rocks. *Earth Planet. Sci. Lett.* **105**, 543–553.

Demouchy S., Jacobsen S. D., Gaillard F. and Stern C. R. (2006) Rapid magma ascent recorded by water diffusion profiles in olivine from Earth's mantle. *Geology* **34**, 429–432.

Dixon J. E., Dixon T. H., Bell D. R. and Malservisi R. (2004) Lateral variation in upper mantle viscosity: role of water. *Earth Planet. Sci. Lett.* **222**, 451–467.

Dottin J. W., Labidi J., Farquhar J., Piccoli P. M., Liu M.-C. and McKeegan K. D. (2018) Evidence for oxidation at the base of the nakhlite pile by reduction of sulfate salts at the time of lava emplacement. *Geochim. Cosmochim. Acta* **239**, 186–197.

Drake M. J. (2005) Origin of water in the terrestrial planets. *Meteor. Planet. Sci.* **40**, 519–527.

Dudley J.-M., Peslier A. H. and Hervig R. (2019) Hydrogen isotope fractionation during impact degassing of pyroxene and maskelynite in shergottite Larkman Nunatak 06319. *Lunar Planet. Sci. Conf The Woodlands, TX*.

Dyar D. (2003) Ferric iron in SNC meteorites as determined by Mössbauer spectroscopy: implications for martian landers and martian oxygen fugacity. *Meteor. Planet. Sci.* **38**, 1733–1752.

Dyar M. D., Treiman A. H., Pieters C. M., Hiroi T., Lane M. D. and O'Connor V. (2005) MIL03346, the most oxidized Martian meteorite: a first look at spectroscopy, petrography, and mineral chemistry. *J. Geophys. Res.* **110**, E09005.

Elkins-Tanton L. T. (2008) Linked magma ocean solidification and atmospheric growth for Earth and Mars. *Earth Planet. Sci. Lett.* **271**, 181–191.

Elkins-Tanton L. T., Parmentier E. M. and Hess P. C. (2003) Magma ocean fractional crsytallization and cumulate overturn in terrestrial planets: implications for Mars. *Meteor. Planet. Sci.* **38**, 1753–1771.

Eugster O., Busemann H., Lorenzetti S. and Terribilini D. (2002) Ejection ages from krypton-81-krypton-83 dating and pre-atmospheric sizes of martian meteorites. *Meteor. Planet. Sci.* **37**, 1345–1360.

Eugster O., Herzog G. F., Marti K. and Caffee M. W. (2006) Irradiation records, cosmic-ray exposure ages, and transfer times of meteorites. In *Meteorites and the early Solar System II* (eds. D. S. Lauretta and H. Y. McSween). The University of Arizona Press, Tucson, AZ, pp. 829–851.

Farmer C. B., Davies D. W. and Laporte D. D. (1976) Mars - northern summer ice cap -water-vapor observations from Viking 2. *Science* **194**, 1339–1341.

Fedorova A. A., Korablev O. I., Bertaux J. L., Rodin A. V., Montmessin F., Belyaev D. A. and Reberac A. (2009) Solar infrared occultation observations by SPICAM experiment on Mars-Express: simultaneous measurements of the vertical distributions of H_2O, CO_2 and aerosol. *Icarus* **200**, 96–117.

Fergason R. L., Christensen P. R., Bell J. F., Golombek M. P., Herkenhoff K. E. and Kieffer H. H. (2006) Physical properties of the Mars Exploration Rover landing sites as inferred from Mini-TES–derived thermal inertia. *J. Geophys. Res.: PLanets* **111**, n/a-n/a.

Férot A. and Bolfan-Casanova N. (2012) Water storage capacity in olivine and pyroxene to 14 GPa: implications for the water content of the Earth's upper mantle and nature of seismic discontinuities. *Earth Planet. Sci. Lett.* **349–350**, 218–230.

Ferriss E., Plank T. and Walker D. (2016) Site-specific hydrogen diffusion rates during clinopyroxene dehydration. *Cont. Min. Pet.* **171**, 1–24.

Filiberto J. and Treiman A. H. (2009) Martian magmas contained abundant chlorine, but little water. *Geology* **37**, 1087–1090.

Filiberto J., Treiman A. H., Giesting P. A., Goodrich C. A. and Gross J. (2014) High-temperature chlorine-rich fluid in the martian crust: a precursor to habitability. *Earth Planet. Sci. Lett.* **401**, 110–115.

Floran R. J., Prinz M., Hlava P. F., Keil K., Nehru C. E. and Hinthorne J. R. (1978) The Chassigny meteorite: a cumulate dunite with hydrous amphibole-bearing melt inclusions. *Geochim. Cosmochim. Acta* **42**, 1213–1229.

Franz H. B., Kim S.-T., Farquhar J., Day J. M. D., Economos R. C., McKeegan K. D., Schmitt A. K., Irving A. J., Hoek J. and

Dottin () Isotopic links between atmospheric chemistry and the deep sulphur cycle on Mars. *Nature* **508**, 364–368.

Fritz J. and Greshake A. (2009) High-pressure phases in an ultramafic rock from Mars. *Earth Planet. Sci. Lett.* **288**, 619–623.

Fritz J., Artemieva N. and Greshake A. (2005a) Ejection of Martian meteorites. *Meteor. Planet. Sci.* **40**, 1393–1411.

Fritz J., Greshake A. and Stöffler D. (2005b) Micro-Raman spectroscopy of plagioclase and maskelynite in martian meteorites: evidence of progressive shock metamorphism. *Antarct. Meteorite Res.* **18**, 98–116.

Geiss J. and Gloeckler G. (1998) Abundances of deuterium and helium-3 in the protosolar cloud. *Space Sci. Rev.* **84**, 239–250.

Giesting P. A. and Filiberto J. (2016) The formation environment of potassic-chloro-hastingsite in the nakhlites MIL 03346 and pairs and NWA 5790: insights from terrestrial chloro-amphibole. *Meteor. Planet. Sci.* **51**, 2127–2153.

Giesting P. A., Schwenzer S. P., Filiberto J., Starkey N. A., Franchi I. A., Treiman A. H., Tindle A. G. and Grady M. M. (2015) Igneous and shock processes affecting chassignite amphibole evaluated using chlorine/water partitioning and hydrogen isotopes. *Meteor. Planet. Sci.* **50**, 433–460.

Gilmour J. D., Whitby J. A. and Turner G. (2001) Disentangling xenon components in Nakhla: martian atmosphere, spallation and martian interior. *Geochim. Cosmochim. Acta* **65**, 343–354.

Gonfiantini R. (1978) Standards for stable isotope measurements in natural compounds. *Nature* **271**, 534–536.

Gooding J. L., Wentworth S. J. and Zolensky M. E. (1991) Aqueous alteration of the Nakhla meteorite. *Meteoritics* **26**, 135–143.

Grant K. J., Kohn S. C. and Brooker R. A. (2006) Solubility and partitioning of water in synthetic forsterite and enstatite in the system $MgO-SiO_2-H_2O\pm Al_2O_3$. *Cont. Min. Pet.* **151**, 651–664.

Greenwood J. P., Itoh S., Sakamoto N., Vicenzi E. P. and Yurimoto H. (2008) Hydrogen isotope evidence for loss of water from Mars through time. *Geophys. Res. Lett.* **35**, L05203.

Grove, T. L. and Bence, A. E. (1977) Experimental study of pyroxene-liquid interaction in quartz-nomative basalt 15597. In Eighth Lunar and Planetary Conference, Houston, TX. pp. 1549–1579.

Halliday A. N. (2013) The origins of volatiles in the terrestrial planets. *Geochim. Cosmochim. Acta* **105**, 146–171.

Hallis L. J. (2017) D/H ratios of the inner Solar System. *Phil. Trans. R. Soc.* **A**, 375.

Hallis L. J. and Taylor G. J. (2011) Comparison of the four Miller Range nakhlites, MIL 03346, 090030, 090032 and 090136: textural and compositional observations of primary and secondary mineral assemblages. *Meteor. Planet. Sci.* **46**, 1787–1803.

Hallis L. J., Taylor G. J., Nagashima K. and Huss G. R. (2012a) Magmatic water in the martian meteorite Nakhla. *Earth Planet. Sci. Lett.* **359–360**, 84–92.

Hallis L. J., Taylor G. J., Nagashima K., Huss G. R., Needham A. W., Grady M. M. and Franchi I. A. (2012b) Hydrogen isotope analyses of alteration phases in the nakhlite martian meteorites. *Geochim. Cosmochim. Acta* **97**, 105–119.

Hallis L. J., Ishii H. A., Bradley J. P. and Taylor G. J. (2014) Transmission electron microscope analyses of alteration phases in martian meteorite MIL 090032. *Geochim. Cosmochim. Acta* **134**, 275–288.

Hallis L. J., Huss G. R., Nagashima K., Taylor G. J., Halldórsson S. A., Hilton D. R., Motti M. J. and Meech K. J. (2015) Evidence for primordial water in Earth's deep mantle. *Science* **350**, 795–797.

Hallis L. J., Huss G. R., Nagashima K., Taylor G. J., Stöffler D., Smith C. L. and Lee M. R. (2017) Effects of shock and Martian

alteration on Tissint hydrogen isotope ratios and water content. *Geochim. Cosmochim. Acta* **200**, 280–294.

Hartogh P., Lis D. C., Bockelee-Morvan D., de Val-Borro M., Biver N., Kuppers M., Emprechtinger M., Bergin E. A., Crovisier J., Rengel M., Moreno R., Szutowicz S. and Blake G. A. (2011) Ocean-like water in the Jupiter-family comet 103P/Hartley 2. *Nature* **478**, 218–220.

Harvey R. P. and McSween H. Y. J. (1992) Petrogenesis of the Nakhlite meteorites: evidence from cumulate mineral zoning. *Geochim. Cosmochim. Acta* **56**, 1655–1663.

Hashizume K., Chaussidon M., Marty B. and Robert F. (2000) Solar wind record on the Moon: deciphering presolar from planetary nitrogen. *Science* **290**, 1142–1145.

Hauri E. H., Gaetani G. A. and Green T. H. (2006) Partitioning of water during melting of the Earth's upper mantle at H_2O-undersaturated conditions. *Earth Planet. Sci. Lett.* **248**, 715–734.

Hercule S. and Ingrin J. (1999) Hydrogen in diopside: diffusion, kinetics of extraction-incorporation, and solubility. *Am. Mineral.* **84**, 1577–1587.

Herd C. D. K. (2003) The oxygen fugacity of olivine-phyric martian basalts and the components within the mantle and crust of Mars. *Meteor. Planet. Sci.* **38**, 1793–1805.

Hier-Majumder S. and Hirschmann M. M. (2017) The origin of volatiles in the Earth's mantle. *Geochem. Geophys. Geosyst.* **18**, 3078–3092.

Hirschmann M. M., Aubaud C. and Withers A. C. (2005) Storage capacity of H_2O in nominally anhydrous minerals in the upper mantle. *Earth Planet. Sci. Lett.* **236**, 167–181.

Hofmeister A. M. (2004) Enhancement of radiative transfer in the upper mantle by OH- in minerals. *Phys. Earth Planet. Int.* **146**, 483–495.

Horner J., Mousis O. and Hersant F. (2007) Constraints on the Formation Regions of Comets from their D: H Ratios. *Earth, Moon, and Planets* **100**, 43–56.

Hu S., Lin Y., Zhang J., Hao J., Feng L., Xu L., Yang W. and Yang J. (2014) NanoSIMS analyses of apatite and melt inclusions in the GRV 020090 Martian meteorite: hydrogen isotope evidence for recent past underground hydrothermal activity on Mars. *Geochim. Cosmochim. Acta* **140**, 321–333.

Imae N., Ikeda Y. and Kojima H. (2005) Petrology of the Yamato nakhlites. *Meteor. Planet. Sci.* **40**, 1581–1598.

Ingrin J. and Blanchard M. (2006) Diffusion of hydrogen in minerals. In *Water in nominally anhydrous minerals* (eds. H. Keppler and J. R. Smyth). Mineralogical Society of America, Chantilly, VA, pp. 291–320.

Jambon A., Sautter V., Barrat J. A., Gattacceca J., Rochette P., Boudouma O., Badia D. and Devouard B. (2016) Northwest Africa 5790: revisiting nakhlite petrogenesis. *Geochim. Cosmochim. Acta* **190**, 191–212.

Johnson E. A. and Rossman G. R. (2004) A survey of hydrous species and concentrations in igneous feldspars. *Am. Mineral.* **89**, 586–600.

Keller L. P. and McKay D. S. (1997) The nature and origin of rims on linar soil grains. *Geochim. Cosmochim. Acta* **61**, 2331–2341.

Kerridge J. F. (1985) Carbon, hydrogen and nitrogen in carbonaceous chondrites: abundances and isotopic compositions in bulk samples. *Geochim. Cosmochim. Acta* **49**, 1707–1714.

Kiefer W. S. and Li Q. (2016) Water undersaturated mantle plume volcanism on present-day Mars. *Meteor. Planet. Sci.* **51**, 1993–2010.

Kohlstedt D. L., Keppler H. and Rubie D. C. (1996) Solubility of water in the α, β and γ phases of $(Mg, Fe)_2SiO_4$. *Cont. Min. Pet.* **123**, 345–357.

Korochantseva E. V., Schwenzer S. P., Buikin A. I., Hopp J., Ott U. and Trieloff M. (2011) ^{40}Ar-^{39}Ar and cosmic-ray exposure

ages of nakhlites—Nakhla, Lafayette, Governador Valadares—and Chassigny. *Meteor. Planet. Sci.* **46**, 1397–1417.

Lammer H., Chassefière E., Karatekin Ö., Morschhauser A., Niles P. B., Mousis O., Odert P., Möstl U. V., Breuer D., Dehant V., Grott M., Gröller H., Hauber E. and Pham L. B. S. (2013) Outgassing history and escape of the Martian atmosphere and water inventory. *Space Sci. Rev.* **174**, 113–154.

Lécuyer C., Gillet P. and Robert F. (1998) The hydrogen isotope composition of seawater and the global water cycle. *Chem. Geol.* **145**, 249–261.

Lee M. R., Tomkinson T., Mark D. F., Stuart F. M. and Smith C. L. (2013) Evidence for silicate dissolution on Mars from the Nakhla meteorite. *Meteor. Planet. Sci.* **48**, 224–240.

Lemaire C., Kohn S. C. and Brooker R. A. (2004) The effect of silica activity on the incorporation mechanisms of water in synthetic forsterite: a polarized infrared spectroscopic study. *Cont. Min. Pet.* **147**, 48–57.

Lentz R. C. F., McCoy T. J., Collins L. E., Corrigan C. M., Benedix G. K., Taylor G. J. and Harvey R. P. (2011) Theo's Flow, Ontario, Canada: a terrestrial analog for the Martian nakhlite meteorites. *Geol. Soc. Am. Sp. Papers* **483**, 263–277.

Leshin L. A., Epstein S. and Stolper E. (1996) Hydrogen isotope geochemistry of SNC meteorites. *Geochim. Cosmochim. Acta* **60**, 2635–2650.

Leshin L. A., Mahaffy P. R., Webster C. R., Cabane M., Coll P., Conrad P. G., Archer P. D., Atreya S. K., Brunner A. E., Buch A., Eigenbrode J. L., Flesch G. J., Franz H. B., Freissinet C., Glavin D. P., McAdam A. C., Miller K. E., Ming D. W., Morris R. V., Navarro-González R., Niles P. B., Owen T., Pepin R. O., Squyres S., Steele A., Stern J. C., Summons R. E., Sumner D. Y., Sutter B., Szopa C., Teinturier S., Trainer M. G., Wray J. J., Grotzinger J. P. and Team M. S. (2013) Volatile, isotope, and organic analysis of martian fines with the mars curiosity rover. *Science* **341**.

Libowitzky E. and Beran A. (2004) IR spectroscopic characterization of hydrous species in minerals. In *Spectroscopic Methods in Mineralogy* (eds. A. Beran and E. Libowitzky). European Mineralogical Union, pp. 227–279.

Libowitzky E. and Beran A. (2006) The structure of hydrous species in nominally anhydrous minerals: Information from polarized IR spectroscopy. In *Water in Nominally Anhydrous Minerals* (eds. H. Keppler and J. R. Smyth). Mineralogical Society of America, Chantilly, VA, pp. 29–52.

Libowitzky E. and Rossman G. R. (1996) Principles of quantitative absorbance measurements in anisotropic crystals. *Phys. Chem. Min.* **23**, 319–327.

Liu J., Xia Q.-K., Deloule E., Ingrin J., Chen H. and Feng M. (2015) Water content and oxygen isotopic composition of alkali basalts from the Taihang Mountains, China: recycled oceanic components in the mantle source. *J. Petrol.* **56**, 681–702.

Liu Y., Ma C., Beckett J. R., Chen Y. and Guan Y. (2016) Rare-earth-element minerals in martian breccia meteorites NWA 7034 and 7533: implications for fluid–rock interaction in the martian crust. *Earth Planet. Sci. Lett.* **451**, 251–262.

Liu Y., Chen Y., Guan Y., Ma C., Rossman G. R., Eiler J. M. and Zhang Y. (2018) Impact-melt hygrometer for Mars: The case of shergottite Elephant Moraine (EETA) 79001. *Earth Planet. Sci. Lett.* **490**, 206–215.

Lloyd A. S., Ferriss E., Ruprecht P., Hauri E. H., Jicha B. R. and Plank T. (2016) An assessment of clinopyroxene as a recorder of magmatic water and magma ascent rate. *J. Petrol.* **57**, 1865–1886.

Longhi J. and Pan V. (1989) The parent magmas of the SNC meteorites. In *19th Lunar and Planetary Conference Houston, TX*, pp. 451–464.

Longhi J., Walker D. and Hays J. F. (1976) Fe and Mg in plagioclase. In *Lunar Planet. Sci. Conf., Houston, TX*, pp. 1281–1300.

Lorand J. P., Hewins R. H., Remusat L., Zanda B., Pont S., Leroux H., Marinova M., Jacob D., Humayun M., Nemchin A., Grange M., Kennedy A. and Göpel C. (2015) Nickeliferous pyrite tracks pervasive hydrothermal alteration in Martian regolith breccia: a study in NWA 7533. *Meteor. Planet. Sci.* **50**, 2099–2120.

Lowell R. P. and Rona P. A. (2002) Seafloor hydrothermal systems driven by the serpentinization of peridotite. *Geophys. Res. Lett.* **29**, 26-21-26-24.

Lunine J. I., Chambers J., Morbidelli A. and Leshin L. A. (2003) The origin of water on Mars. *Icarus* **165**, 1–8.

Mackwell S. J., Kohlstedt D. L. and Paterson M. S. (1985) The role of water in the deformation of olivine single crystals. *J. Geophys. Res.* **90**, 11319–11333.

Magna T., Day J. M. D., Mezger K., Fehr M. A., Dohmen R., Aoudjehane H. C. and Agee C. B. (2015) Lithium isotope constraints on crust–mantle interactions and surface processes on Mars. *Geochim. Cosmochim. Acta* **162**, 46–65.

Mane P., Hervig R., Wadhwa M., Garvie L. A. J., Balta J. B. and McSween H. Y. (2016) Hydrogen isotopic composition of the Martian mantle inferred from the newest Martian meteorite fall. *Tissint. Meteor. Planet. Sci.* **51**, 2073–2091.

Marti K. and Mathew K. J. (2004) Martian mantle signatures in Yamato nakhlites. *Antarct. Meteorite Res.* **17**, 117–131.

Marty B., Chaussidon M., Wiens R. C., Jurewicz A. J. G. and Burnett D. S. (2011) A ^{15}N-poor isotopic composition for the Solar System as shown by Genesis solar wind samples. *Science* **332**, 1533–1536.

Mathew K. J. and Marti K. (2002) Martian atmospheric and interior volatiles in the meteorite Nakhla. *Earth Planet. Sci. Lett.* **199**, 7–20.

Mathew K. J. and Marti K. (2005) Evolutionary trends in volatiles of the nakhlite source region of Mars. *J. Geophys. Res.* **110**, 11–18, E12S05.

Mathew K. J., Marty B., Marti K. and Zimmermann L. (2003) Volatiles (nitrogen, noble gases) in recently discovered SNC meteorites, extinct radioactivities and evolution. *Earth Planet. Sci. Lett.* **214**, 27–42.

McCanta M. C., Elkins-Tanton L. T. and Rutherford M. J. (2009) Expanding the application of the Eu-oxybarometer to the lherzolitic shergottites and nakhlites: implications for the oxidation state heterogeneity of the Martian interior. *Meteor. Planet. Sci.* **44**, 725–745.

McCubbin F. M., Tosca N. J., Smirnov A., Nekvasil H., Steele A., Fries M. and Lindsley D. H. (2009) Hydrothermal jarosite and hematite in a pyroxene-hosted melt inclusion in martian meteorite Miller Range (MIL) 03346: implications for magmatic-hydrothermal fluids on Mars. *Geochim. Cosmochim. Acta* **73**, 4907–4917.

McCubbin F. M., Smirnov A., Nekvasil H., Wang J., Hauri E. and Lindsley D. H. (2010) Hydrous magmatism on Mars: a source of water for the surface and subsurface during the Amazonian. *Earth Planet. Sci. Lett.* **292**, 132–138.

McCubbin F. M., Elardo S. M., Shearer C. K., Smirnov A., Hauri E. H. and Draper D. S. (2013) A petrogenetic model for the comagmatic origin of chassignites and nakhlites: inferences from chlorine-rich minerals, petrology, and geochemistry. *Meteor. Planet. Sci.* **48**, 819–853.

McCubbin F. M., Boyce J. W., Srinivasan P., Santos A. R., Elardo S. M., Filiberto J., Steele A. and Shearer C. K. (2016) Heterogeneous distribution of H_2O in the Martian interior: implications for the abundance of H_2O in depleted and enriched mantle sources. *Meteor. Planet. Sci.* **51**, 2036–2060.

McSween H. Y. (2015) Petrology on Mars. *Am. Mineral.* **100**, 2380–2395.

McSween, Jr., H. Y., Grove T. L., Lentz R. C., Dann J. C., Holzheid A. H., Riciputi L. R. and Ryan C. G. (2001) Geochemical evidence for magmatic water within Mars from pyroxenes in the Shergotty meteorite. *Nature* **409**, 487–490.

Médard E. and Grove T. L. (2006) Early hydrous melting and degassing of the martian interior. *J. Geophys. Res.* **111**, E11003.

Merlivat L., Lelu M. and Neif G. (1976) *Spallation deuterium in rock 70215.* Lunar Planet. Sci. Conf, Houston, TX, pp. 649–658.

Michael P. (1995) Regionally distinctive sources of depleted MORB: evidence from trace elements and H$_2$O. *Earth Planet. Sci. Lett.* **131**, 301–320.

Mikouchi T., Koizumi E., Monkawa A., Ueda Y. and Miyamoto M. (2003) Mineralogy and petrology of Yamato 000593: comparison with other Martian meteorites. *Antarct. Meteorite Res.* **16**, 34–57.

Miller G. H., Rossman G. R. and Harlow G. E. (1987) The natural occurrence of hydroxide in olivine. *Phys. Chem. Min.* **14**, 461–472.

Minitti M. E., Leshin L. A., Dyar D., Ahrens T. J., Guan Y. and Luo S.-N. (2008a) Assessment of shock effects on amphibole water contents and hydrogen isotope compositions: 2. kaersutitic amphibole experiments. *Earth Planet. Sci. Lett.* **266**, 288–302.

Minitti M. E., Rutherford M. C., Taylor B. E., Dyar D. and Schultz P. H. (2008b) Assessment of shock effects on amphibole water contents and hydrogen isotope compositions: 1. amphibolite experiments. *Earth Planet. Sci. Lett.* **266**, 46–60.

Morschhauser A., Grott M. and Breuer D. (2011) Crustal recycling, mantle dehydration, and the thermal evolution of Mars. *Icarus* **212**, 541–558.

Mouginot J., Pommerol A., Beck P., Kofman W. and Clifford S. M. (2012) Dielectric map of the Martian northern hemisphere and the nature of plain filling materials. *Geophys. Res. Lett.* **39**, L02202.

Mysen B. (2013) Hydrogen isotope fractionation between coexisting hydrous melt and silicate-saturated aqueous fluid: an experimental study in situ at high pressure and temperature. *Am. Mineral.* **98**, 376–386.

Nekvasil H., Dondolini A., Horn J., Filiberto J., Long H. and Lindsley D. H. (2004) The origin and evolution of silica-saturated alkalic suites: an experimental study. *J. Petrol.* **45**, 693–721.

Nekvasil H., Filiberto J., McCubbin F. M. and Lindsley D. H. (2007) Alkalic parental magmas for chassignites? *Meteor. Planet. Sci.* **42**, 979–992.

Niles P. B., Michalski J. R., Ming D. W. and Golden D. C. (2017) Elevated olivine weathering rates and sulfate formation at cryogenic temperatures on Mars. *Nat. Commun.* **8**, 998.

Noll P. D., Newman H. E., Leeman W. P. and Ryan J. G. (1996) The role of hydrothermal fluids in the production of subduction zone magmas: evidence from siderophile and chalcophile trace elements and boron. *Geochim. Cosmochim. Acta* **60**, 587–611.

Nyquist L. E., Bogard D. D., Shih C.-Y., Greshake A., Stöffler D. and Eugster O. (2001) Ages and geological histories of martian meteorites. *Space Sci. Rev.* **96**, 105–164.

O'Brien D. P., Walsh K. J., Morbidelli A., Raymond S. N. and Mandell A. V. (2014) Water delivery and giant impacts in the 'Grand Tack' scenario. *Icarus* **239**, 74–84.

O'Leary J. A., Gaetani G. A. and Hauri E. H. (2010) The effect of tetrahedral Al^{3+} on the partitioning of water between clinopyroxene and silicate melt. *Earth Planet. Sci. Lett.* **297**, 111–120.

Orosei R., Jordan R. L., Morgan D. D., Cartacci M., Cicchetti A., Duru F., Gurnett D. A., Heggy E., Kirchner D. L., Noschese R., Kofman W., Masdea A., Plaut J. J., Seu R., Watters T. R. and Picardi G. (2015) Mars Advanced Radar for Subsurface and Ionospheric Sounding (MARSIS) after nine years of operation: a summary. *Planet. Space Sci.* **112**, 98–114.

Owen T., Maillard J. P., de Bergh C. and Lutz B. L. (1988) Deuterium on Mars: the abundance of HDO and the value of D/H. *Science* **240**, 1767.

Park J., Garrison D. H. and Bogard D. D. (2009) ^{39}Ar–^{40}Ar ages of martian nakhlites. *Geochim. Cosmochim. Acta* **73**, 2177–2189.

Peslier A. H. (2010) A review of water contents of nominally anhydrous natural minerals in the mantles of Earth, Mars and the Moon. *J. Volc. Geotherm. Res.* **197**, 239–258.

Peslier A. H. and Bizimis M. (2015) Water in Hawaiian peridotite minerals: a case for a dry metasomatized oceanic mantle lithosphere. *Geochem. Geophys. Geosys.* **16**, 1–22.

Peslier A. H. and Luhr J. F. (2006) Hydrogen loss from olivines in mantle xenoliths from Simcoe (USA) and Mexico: Mafic alkalic magma ascent rates and water budget of the sub-continental lithosphere. *Earth Planet. Sci. Lett.* **242**, 302–319.

Peslier A. H., Luhr J. F. and Post J. (2002) Low water contents in pyroxenes from spinel-peridotites of the oxidized, sub-arc mantle wedge. *Earth Planet. Sci. Lett.* **201**, 69–86.

Peslier A. H., Woodland A. B. and Wolff J. A. (2008) Fast kimberlite ascent rates estimated from hydrogen diffusion profiles in xenolithic olivines from Southern Africa. *Geochim. Cosmochim. Acta* **72**, 2711–2722.

Peslier A. H., Hnatyshin D., Herd C. D. K., Walton E. L., Brandon A. D., Lapen T. J. and Shafer J. T. (2010) Crystallization, melt inclusion, and redox history of a martian meteorite: olivine-phyric shergottite Larkman Nunatak 06319. *Geochim. Cosmochim. Acta* **74**, 4543–4576.

Peslier A. H., Woodland A. B., Bell D. R., Lazarov M. and Lapen T. J. (2012) Metasomatic control of water contents in the Kaapvaal cratonic mantle. *Geochim. Cosmochim. Acta* **97**, 213–246.

Peslier A. H., Bizimis M. and Matney M. (2015) Water disequilibrium in olivines from Hawaiian peridotites: recent metasomatism, H diffusion and magma ascent rates. *Geochim. Cosmochim. Acta* **154**, 98–117.

Peslier A. H., Schönbächler M. and Busemann H. (2017) Water in the Earth's interior: distribution and origin. *Space Sci. Rev.* **212**, 743–811.

Piani L., Robert F. and Remusat L. (2015) Micron-scale D/H heterogeneity in chondrite matrices: a signature of pristine Solar System water? *Earth Planet Sci. Lett.* **415**, 154–164.

Pommier A., Grove T. L. and Charlier B. (2012) Water storage and early hydrous melting of the martian mantle. *Earth Planet. Sci. Lett.* **333–334**, 272–281.

Raymond S. N. and Izidoro A. (2017) Origin of water in the inner Solar System: planetesimals scattered inward during Jupiter and Saturn's rapid gas accretion. *Icarus* **297**, 134–148.

Reedy R. C. (1981) Cosmic-ray produced stable nuclides: various production rates and their implications. In *Lunar Planet. Sci. Conf., Houston, TX*, pp. 1809–1823.

Reedy R. C., Arnold J. R. and Lal D. (1983) Cosmic-ray record in Solar System matter. *Ann. Rev. Nucl. Part. Sci.* **33**, 505–537.

Reid A. M. and Bunch T. E. (1975) The nakhlites, Part II: where, when and how. *Meteoritics* **10**, 317–324.

Richter F., Watson B., Chaussidon M., Mendybaev R. and Ruscitto D. M. (2014) Lithium isotope fractionation by diffusion in minerals. Part 1: pyroxenes. *Geochim. Cosmochim. Acta* **126**, 352–370.

Richter F., Chaussidon M., Mendybaev R. and Kite E. (2016) Reassessing the cooling rate and geologic setting of Martian meteorites MIL 03346 and NWA 817. *Geochim. Cosmochim. Acta* **182**, 1–23.

Rodin A. V., Korablev O. I. and Moroz V. I. (1997) Vertical distribution of water in the near-equatorial troposphere of Mars: water vapor and clouds. *Icarus* **125**, 212–229.

Roskosz M., Laurent B., Leroux H. and Remusat L. (2016) Experimental investigation of irradiation-driven hydrogen isotope fractionation in analogs of protoplanetary hydrous silicate dust. *Astrophys. J.* **832**, 55.

Roskosz M., Deloule E., Ingrin J., Depecker C., Laporte D., Merkel S., Remusat L. and Leroux H. (2018) Kinetic D/H fractionation during hydration and dehydration of silicate glasses, melts and nominally anhydrous minerals. *Geochim. Cosmochim. Acta* **233**, 14–32.

Sarafian E., Evans R. L., Collins J. A., Elsenbeck J., Gaetani G. A., Gaherty J. B., Hirth G. and Lizarralde D. (2015) The electrical structure of the central Pacific upper mantle constrained by the NoMelt experiment. *Geochem. Geophys. Geosys.* **16**, 1115–1132.

Scholten L., Watenphul A., Beermann O., Testemale D., Ames D. and Schmidt C. (2018) Nickel and platinum in high-temperature H2O + HCl fluids: implications for hydrothermal mobilization. *Geochim. Cosmochim. Acta* **224**, 187–199.

Seiff A. and Kirk D. B. (1977) Structure of the atmosphere of Mars in summer at mid-latitudes. *J. Geophys. Res.* **82**, 4364–4378.

Sekine T., Meng C., Zhu W. and He H. (2012) Direct evidence for decomposition of antigorite under shock loading. *J. Geophys. Res.* **117**, B03212.

Sekine T., Kimura T., Kobayashi T. and Mashimo T. (2015) Dynamic water loss of antigorite by impact process. *Icarus* **250**, 1–6.

Sharp, Z. (2017a) Principles of stable isotopic geochemistry, 2nd ed.

Sharp Z. D. (2017b) Nebular ingassing as a source of volatiles to the Terrestrial planets. *Chem. Geol.* **448**, 137–150.

Sharp T. G. and DeCarli P. S. (2006) Shock effects in meteorites. In *Meteorites and the early Solar System II* (eds. D. S. Lauretta and H. Y. McSween). The University of Arizona Press, Tucson, AZ, pp. 653–677.

Sharp Z. D., McCubbin F. M. and Shearer C. K. (2013) A hydrogen-based oxidation mechanism relevant to planetary formation. *Earth Planet. Sci. Lett.* **380**, 88–97.

Shaw A. M., Hauri E. H., Behn M. D., Hilton D. R., McPherson C. G. and Sinton J. M. (2012) Long-term preservation of slab signatures in the mantle inferred from hydrogen isotopes. *Nat. Geo.* **5**, 224–228.

Shearer C. K., Messenger S., Sharp Z. D., Burger P. V., Nguyen A. N. and McCubbin F. M. (2018) Distinct chlorine isotopic reservoirs on Mars. implications for character, extent and relative timing of crustal interactions with mantle-derived magmas, evolution of the martian atmosphere, and the building blocks of an early Mars. *Geochim. Cosmochim. Acta* **234**, 24–36.

Skogby H., Bell D. R. and Rossman G. R. (1990) Hydroxide in pyroxene: variations in the natural environment. *Am. Mineral.* **75**, 764–774.

Sobolev A. V. and Chaussidon M. (1996) H2O concentrations in primary melts from supra-subduction zones and mid-ocean ridges: implications for H2O storage and recycling in the mantle. *Earth Planet. Sci. Lett.* **137**, 45–55.

Sparks R. S. J., Barclay J., Jaupart C., Mader H. M. and Phillips J. C. (1994) Physical aspects of magmatic degassing I. Experimental and theoretical constraints on vesiculation. In *Volatiles in Magmas* (eds. M. R. Carroll and J. R. Holloway). Mineralogical Society of America, Washington D.C., pp. 413–446.

Stephant A., Hervig R., Bose M. and Wadhwa M. (2016) D/H ratios and water contents in eucrite minerals: implications for the source and abundance of water on Vesta. In *, 79th Annual Meeting of the Meteoritical Society*. Lunar and Planetary Institute, Berlin, p. 1921.

Stephant A., Remusat L. and Robert F. (2017) Water in type I chondrules of Paris CM chondrite. *Geochim. Cosmochim. Acta* **199**, 75–90.

Stephant A., Garvie L. A. J., Mane P., Hervig R. and Wadhwa M. (2018) Terrestrial exposure of a fresh Martian meteorite causes rapid changes in hydrogen isotopes and water concentrations. *Nat. Sci. Reports* **8**, 12385.

Suzuoki T. and Epstein S. (1976) Hydrogen isotope fractionation between OH-bearing minerals and water. *Geochim. Cosmochim. Acta* **40**, 1229–1240.

Szymanski A., Brenker F. E., Palme H. and El Goresy A. (2010) High oxidation state during formation of Martian nakhlites. *Meteor. Planet. Sci.* **45**, 21–31.

Taylor H. P. and Sheppard S. M. F. (1986) Igneous rocks: I. Processes of isotopic fractionation and isotopic systematics. In *Stable isotopes* (eds. J. W. Valley, H. P. Taylor and J. R. O'Neil). Mineralogical Society of America, pp. 227–272.

Tenner T. J., Hirschmann M. M., Withers A. C. and Hervig R. L. (2009) Hydrogen partitioning between nominally anhydrous upper mantle minerals and melt between 3 and 5 GPa and applications to hydrous peridotite partial melting. *Chem. Geol.* **262**, 42–56.

Terribilini D., Busemann H. and Eugster O. (2000) Krypton-81-Krypton CRE ages of martian meteorites including the new shergottite Los Angeles. *Meteor. Planet Sci* **35**.

Treiman A. H. (2005) The nakhlite meteorites: augite-rich igneous rocks from Mars. *Chem. Erde* **65**, 203–270.

Treiman A. H. and Irving A. J. (2008) Petrology of martian meteorite Northwest Africa 998. *Meteor. Planet. Sci.* **43**, 829–854.

Treiman A. H., Dyar M. D., McCanta M., Pieters M., Hiroi T., Lane M. D. and Bishop J. (2007) Martian dunite NWA 2737: petrographic constraints, geological history, shock events, and olivine color. *J. Geophys. Res.* **112**, E04002.

Tyburczy J. A. and Ahrens T. J. (1988) Dehydration kinetics of shocked serpentine. In *19th Lunar and Planetary Science Conference*. Cambridge University Press, Houston, TX, p. 1427.

Tyburczy J. A., Krishnamurthy R. V., Epstein S. and Ahrens T. J. (1990) Impact-induced devolitization and hydrogen isotopic fractionation of serpentine: implications for planetary accretion. *Earth Planet. Sci. Lett.* **98**, 245–260.

Udry A. and Day J. M. D. (2018) 1.34 billion-year-old magmatism on Mars evaluated from the co-genetic nakhlite and chassignite meteorites. *Geochim. Cosmochim. Acta* **238**, 292–315.

Udry A., McSween J. H. Y., Lecumberri-Sanchez P. and Bodnar R. J. (2012) Paired nakhlites MIL 090030, 090032, 090136, and 03346: insights into the Miller Range parent meteorite. *Meteor. Planet. Sci.* **47**, 1575–1589.

Usui T., McSween, Jr., H. Y. and Floss C. (2008) Petrogenesis of olivine-phyric shergottite Yamato 980459, revisited. *Geochim. Cosmochim. Acta* **72**, 1711–1730.

Usui T., Alexander C. M. O. D., Wang J., Simon J. I. and Jones J. H. (2012) Origin of water and mantle-crust interactions on Mars inferred from hydrogen isotopes and volatile element abundances of olivine-hosted melt inclusions of primitive shergottites. *Earth Planet. Sci. Lett.* **357–358**, 119–129.

Usui T., Alexander C. M. O. D., Wang J., Simon J. I. and Jones J. H. (2015) Meteoritic evidence for a previously unrecognized hydrogen reservoir on Mars. *Earth Planet. Sci. Lett.* **410**, 140–151.

Villanueva G. L., Mumma M. J., Novak R. E., Käufl H. U., Hartogh P., Encrenaz T., Tokunaga A., Khayat A. and Smith M. D. (2015) Strong water isotopic anomalies in the martian atmosphere: probing current and ancient reservoirs. *Science* **348**, 218–221.

Wadhwa M. (2001) Redox state of Mars' upper mantle and crust from Eu anomalies in shergottite pyroxenes. *Science* **291**, 1527–1530.

Wadhwa M. and Crozaz G. (1995) Trace and minor elements in minerals of nakhlites and Chassigny: clues to their petrogenesis. *Geochim. Cosmochim. Acta* **59**, 3629–3645.

Wadhwa M., Crozaz G. and Barrat J. A. (2004) Trace element distributions in the Yamato 000593/000749, NWA 817 and NWA 998 nakhlites: implications for their petrogenesis and mantle source on Mars. *Antarct. Meteorite Res.* **17**, 97–116.

Walsh K. J., Morbidelli A., Raymond C. A., O'Brien D. P. and Mandell A. M. (2011) A low mass for Mars from Jupiter's early gas-driven migration. *Nature* **475**, 206–209.

Watson L. L., Hutcheon I. D., Epstein S. and Stolper E. M. (1994) Water on Mars: clues from deuterium/hydrogen and water contents of hydrous phases in SNC meteorites. *Science* **265**, 86–90.

Webster C. R., Mahaffy P. R., Flesch G. J., Niles P. B., Jones J. H., Leshin L. A., Atreya S. K., Stern J. C., Christensen L. E., Owen T., Franz H., Pepin R. O., Steele A. and Team M. S. L. S. (2013) Isotope ratios of H, C, and O in CO_2 and H_2O of the Martian atmosphere. *Science* **341**, 260–263.

Weis F. A., Bellucci J. J., Skogby H., Stalder R., Nemchin A. A. and Whitehouse M. J. (2017) Water content in the Martian mantle: a Nakhla perspective. *Geochim. Cosmochim. Acta* **212**, 84–98.

Withers A. C., Hirschmann M. M. and Tenner T. J. (2011) The effect of Fe on olivine H_2O storage capacity: consequences for H_2O in the martian mantle. *Am. Mineral.* **96**, 1039–1053.

Xia Q.-K., Liu J., Liu S.-C., Kovács I., Feng M. and Dang L. (2013) High water content in Mesozoic primitive basalts of the North China Craton and implications on the destruction of cratonic mantle lithosphere. *Earth Planet. Sci. Lett.* **361**, 85–97.

Yang L., Ciesla F. J. and Alexander C. M. O. D. (2013) The D/H ratio of water in the solar nebula during its formation and evolution. *Icarus* **226**, 256–267.

Yang X., Liu D. and Xia Q.-K. (2014) CO_2-induced small water solubility in olivine and implications for properties of the shallow mantle. *Earth Planet. Sci. Lett.* **403**, 37–47.

Yung Y. L., Wen J.-S., Pinto J. P., Allen M. B., Pierce K. K. and Paulson S. (1988) HDO in the martian atmosphere: implications for the abundance of crustal water. *Icarus* **76**, 146–159.

Zuber M. T., Solomon S. C., Phillips R. J., Smith D. E., Tyler G. L., Aharonson O., Balmino G., Banerdt W. B., Head, III, J. W., Johnson C. L., Lemoine F. G., McGovern P. J., Neumann G. A., Rowlands D. D. and Zhong S. (2000) Internal structure and early thermal evolution of Mars from Mars Global Surveyor topography and gravity. *Science* **287**, 1788–1793.

Associate editor: James M.D. Day